Modified Newton methods for solving fully monolithic phase-field quasi-static brittle fracture propagation

Thomas Wick

Centre de Mathématiques Appliquées
École Polytechnique
Université Paris-Saclay
91128 Palaiseau, France

Modified Newton methods for solving fully monolithic phase-field quasi-static brittle fracture propagation

Thomas Wick[a,1]

[a]Centre de Mathématiques Appliquées, École Polytechnique, Université Paris-Saclay, 91128 Palaiseau, France

Abstract

Our goal in this work is to develop and compare modified Newton methods for fully monolithic quasi-static brittle phase-field fracture propagation. In variational phase-field fracture, a smoothed phase-field indicator variable denoting the crack path is coupled to elasticity. Moreover, a crack irreversibility condition is incorporated. To develop a fully monolithic scheme is an extremely challenging task since the underlying problem is non-convex and the Jacobian of Newton's method is indefinite. To split the problem and using alternating minimization, thus a partitioned approach, is a possible resort. However, there a good reasons to consider monolithic approaches such as for example robustness and efficiency. Although an error-oriented Newton method can cope with a larger variety of configurations, it appears that this method is not always robust and also not always efficient. Inspired by nonlinear flow problems, as alternative, we develop a modified Newton scheme in which globalization is based on a dynamic modification of the Jacobian matrix rather than utilizing line-search or trust-region strategies. This variation switches smoothly between full Newton and Newton-like steps. In several 2D and 3D numerical examples, all of them with different characteristic features, our modified Newton solver is compared to a backtracking line-search Newton method, another line-search method monitoring the global energy and allowing for negative curvatures, and to already published results of an error-oriented version. These computations also include further modifications of Newton's method and detailed discussions why certain schemes either work or fail. Revisiting all findings, the main outcome of this paper is that the modified Newton scheme with Jacobian modification is currently the only method that works in a robust and efficient way for all provided examples, whereas line-search schemes or the error-oriented scheme show deficiencies for certain configurations.

Keywords: phase-field fracture propagation; modified Newton's method; Jacobian modification; line-search; inexact augmented Lagrangian; benchmark tests;
2000 MSC: 2010 74R10; 74F10; 65M60; 49M15; 35Q74

1. Introduction

In 1998, Francfort and Marigo [26] introduced a variational approach to Griffith's [30] quasi-static brittle fracture model. A numerical realization of this model was first presented by Bourdin et al. [14]. Using such a variational approach, discontinuities in the displacement field u across the lower-dimensional crack surface are approximated by an auxiliary phase-field function φ based on elliptic (Ambrosio-Tortorelli) functionals [5, 6]. The latter one is a smoothed indicator function, which introduces a diffusive transition zone of size ε between the broken and the unbroken material. The essential aspects of a variational fracture propagation formulation are techniques that must include the resolution of ε with respect to the spatial discretization parameter h, the enforcement of the irreversibility of crack growth, and the robust and efficient numerical solution of the entire problem. To anticipate the topic of this paper, we focus specifically on the last aspect, namely on the nonlinear solution process using Newton's method.

In 2010, Miehe et al. [50, 53] added more physical explanation and modifications to the original model, yielding a so-called phase-field formulation for fracture propagation. Since then, the method has been extended in various

---

directions as attested in papers on various solution techniques [39, 50, 53, 1, 3, 48, 27, 74, 24], isogeometric analysis [12, 11, 34, 4, 33], discontinuous/enriched Galerkin [23, 58], adaptive (spatial) discretizations [18, 19, 8, 72], dynamic fracture [40, 41, 12, 16, 35, 62], ductile/cohesive fracture [66, 4, 2, 64] and recent comparisons with experimental results or extensions to multiphysics fracture [46, 55, 51, 52, 49, 56, 31, 42, 71, 17, 44] to name a few.

Due to the non-convexity of the underlying energy functional, in most approaches, the solution is obtained via iteration between the variables, a so-called alternating minimization [14, 15, 13, 18, 48]. This idea is based on the fact that by fixing one variable, the problem becomes convex in the other unknown. Such a partitioned approach may however need many iterations; see [67, 27]. A quasi-monolithic approach proposed in [32] goes into the same direction by fixing the phase-field variable φ in the most critical term and using an extrapolation in time $\tilde{\varphi}$. In fact, this algorithm seems to be extremely robust and efficient. Thanks to the triangular block structure, the quasi-monolithic approach could be easily treated with an MPI-parallelized preconditioned GMRES solver applied to 2D and 3D settings [32, 43]. With regard to parallelization it is worthy to notice as well [74] in which a GPU parallelization using a partitioned method has been proposed.

It remains an interesting and challenging problem to design a fully monolithic algorithm because the original system is envisaged to be solved without any perturbations introduced by the numerical solution algorithm. This reflects the paradigm that a numerical algorithm should be designed in such a way that as many properties as possible of the continuous problem are conserved - and this is without any doubts the case for monolithic algorithms. However, due to the non-convexity, the Jacobian matrix in Newton's method becomes indefinite and a straightforward solution process is not robust anymore.

Dealing with ill-conditioned matrices (namely the Hessian[1] of the functional to be minimized) in Newton's method is well known in numerical optimization in which non-monotone, non-convex and indefinite systems often arise [61]. A common strategy is to modify the Hessian in such a way that it becomes again positive definite in order to find (at least) a local minimum. Another approach, a special line-search technique, was developed in the 1970's. Here, the authors work on purpose with the 'wrong' Newton direction while using the negative curvature [29, 59]. However, to find the correct balance between (steepest) descent and the negative curvature is difficult (for further comments we refer the reader to the pages 62-63 in [61]).

For quasi-static phase-field fracture, some reliable experiences using monolithic Newton techniques have been recently reported in the literature [67, 27, 73] (a monolithic concept for dynamic phase-field fracture was first presented in [12]). These studies show, however, that the performance (as almost expected) is highly dependent on the problem configuration, material and model parameters. The key is a careful inspection of the underlying Newton method and the hope that special modifications yield solutions. For instance, [27] designed a special line-search algorithm, which monitors the global energy at each Newton step. The stopping criterion is based as usually on a sufficiently small residual (i.e., the first order necessary condition of the energy functional). Furthermore, the authors also developed a concept to detect negative curvatures of the Newton path. Earlier work was done in [67] in which the weak form was augmented with respect to a dissipation-based arc-length procedure in order to avoid a snapback behavior. The most recent work is [73], which employed an error-oriented Newton method (for the basics we refer to [22]) including comparisons to the quasi-monolithic approach from [32].

On the other hand, for nonlinear flow problems, modified Newton schemes have been proposed in [36] and further investigated in [45, 47]. This technique tries to separate bad terms from well-posed terms in the Jacobian matrix and to scale these bad terms in an appropriate manner such that the method dynamically varies between full Newton and a Newton-like procedure[2]. However, employing this approach, classical line search procedures will not be adopted in addition, since they would act in a counter-productive manner [45] (our own numerical experiments in Example 1 in Section 5 substantiate this claim). The main drawback of this modified Newton scheme is the lack of a rigorous convergence result and remains thus an heuristic procedure, which however seems to work very well in practice.

The main novelty of this paper is to apply such modified Newton schemes to fully monolithic phase-field fracture settings. Specifically, we separate the phase-field derivatives in the elasticity equation from the rest of the matrix and introduce a control parameter ω that is updated at each Newton iteration. The main reason to apply this modified Newton scheme is scientific curiosity, but more importantly a true necessity. In fact, we found in [73] in six different

---

[1]On the PDE level, the Hessian is nothing else then the Jacobian matrix. In the rest of the paper we use both terminologies.

[2]For the definition of a Newton-like procedure, we refer to page 22 in [22]. In optimization terminology, this is nothing else than a special form of a Hessian modification (pages 48-56 in [61]).

numerical tests that an error-oriented Newton approach lacked in some cases efficiency and would not work in one of the six tests. From these results, it can be inferred that the developed methodology is not robust for arbitrary configurations.

In this paper, we will indeed observe large variations of the norm of the Newton residual during single Newton iterations. Moreover, we learn that by such a monolithic treatment the coupling is so tight that smallest perturbations yield different crack patterns and extremely fast crack growth. The first observation coincides with the fact that uniqueness cannot be proven for quasi-static phase-field fracture, e.g., [14, 15]. The fast crack growth is instantaneous and much faster than observed in partitioned (alternating minimization) or quasi-monolithic approaches. This clearly shows that numerical algorithms might have a significant impact on the crack growth, the crack path, and the crack (tip) velocity.

Finally, the further investigation of monolithic algorithms remain important not only for the previously discussed reasons, but also for the fact that some studies found that monolithic algorithms are more efficient in comparison to partitioned (i.e., alternating) techniques [27, 67]. Therefore, it is interesting from the computational cost point of view to further develop monolithic schemes. Moreover, for consistent Galerkin formulations used in adjoint-based error estimation and gradient-based optimization, monolithic formulations are necessary. Involving phase-field fracture, first studies with regard to these two last research topics have been recently published in [72] and [60].

The outline of this paper is as follows. In the first Section 2 the notation and the equations are provided. Next in Section 3 several modifications of Newton methods are explained. We provide insight to the characteristic features of the underlying problem in Section 4. Several benchmarks that include mechanics tests and pressurized fractures are consulted in Section 5 to substantiate our algorithmic developments. The paper finishes with detailed conclusions and acknowledgments.

2. Notation and Governing Equations

2.1. Notation

In this section, we introduce the basic notation and the underlying equations. In the following, let $B \subset \mathbb{R}^d, d = 2, 3$ the total domain wherein $C \subset \mathbb{R}^{d-1}$ denotes the fracture and $\Omega \subset \mathbb{R}^d$ is the intact domain. We assume (possibly time-dependent non-homogeneous) Dirichlet conditions on the outer boundary ∂B.
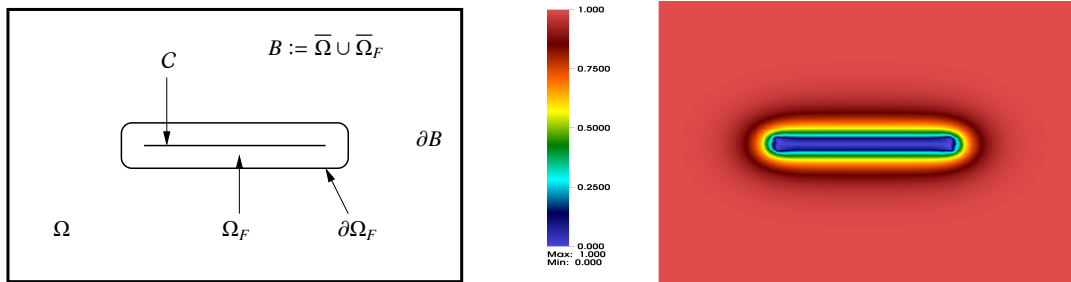
Figure 1: Setup of the notation: the unbroken domain is denoted by Ω and C is the fracture. The latter one is approximated by the domain Ω_F. The half thickness of Ω_F is ε. The fracture boundary is $\partial \Omega_F$ and the outer boundary is ∂B. The corresponding realization using phase-field is shown in the right subfigure. Here, the lower-dimensional fracture ($\varphi = 0$) is approximated with the phase-field variable. The transition zone with $0 < \varphi < 1$ has the thickness of ε on each side of the fracture. Consequently, Ω_F can be represented in terms of φ as defined in (1).

Using a phase-field approach, the one-dimensional fracture C is approximated by $\Omega_F \in \mathbb{R}^d$ with the help of an elliptic (Ambrosio-Tortorelli) functional [5, 6]. Using the phase-field variable φ (introduced in the next subsection 2.2), Ω_F can be defined as:

$$\Omega_F := \{x \in \mathbb{R}^d | \varphi(x) < 1\}. \tag{1}$$

3

For fracture formulations posed in a variational setting, this has been first proposed in [14]. The inner fracture boundary is denoted by the smeared ε-dependent boundary $\partial\Omega_F$. We note that the precise location of $\partial\Omega_F$ is of no importance in this work (in contrast to [55, 44]). The reader is referred to Figure 1 for an illustration of the notation. Since $\partial\Omega_F$ depends on ε, the domains Ω and Ω_F are ε-dependent, too. Finally, we denote the L^2 scalar product with $(a, b) := (a, b)_B := \int_B a \cdot b \, dx$ for vectors a, b. For tensor-valued functions A, B, we have $(A, B) := (A, B)_B := \int_B A : B \, dx$.

2.2. Quasi-static phase-field for brittle fracture

We briefly recapitulate the ingredients for a phase-field model for mechanics and pressurized fractures in brittle materials. Such a model is based on the variational/phase-field fracture approach of [26, 14]. Thermodynamically-consistent phase-field techniques using a stress-split into tension and compression have been proposed in [7] and [53].

The previous formulations start with an energy functional $E(u, \varphi)$ (see also Section 3.3) which is minimized with respect to the unknown solution variables $u : B \to \mathbb{R}^d$ (displacements) and a smoothed scalar-valued indicator phase-field function $\varphi : B \to [0, 1]$. The latter one varies in the zone of size ε from 0 (fracture) to 1 (intact material). The first-order necessary condition are the Euler-Lagrange equations, which are obtained by differentiation with respect to the two unknowns u and φ. Adding a pressure $p : B \to \mathbb{R}$ to the Euler-Lagrange equations that acts on the fracture boundary has been formulated and analyzed in [54, 56, 57]. In all the previous fracture models, the physics of the underlying problem ask to enforce a crack irreversibility condition (the crack can never heal) that is an inequality condition in time:

$$\partial_t \varphi \leq 0. \tag{2}$$

Consequently, modeling of fracture evolution problems leads to a variational inequality system, that is always, due to this constraint, quasi-stationary or time-dependent.

The resulting variational formulation is stated in an incremental (i.e., time-discretized) formulation in which the continuous irreversibility constraint is approximated by

$$\varphi \leq \varphi^{old}.$$

Here, φ^{old} will later denote the previous time step solution and φ the current solution. Let $V := H_0^1(B)$ and

$$W_{in} := \{w \in H^1(B) | \, w \leq \varphi^{old} \leq 1 \text{ a.e. on } B\}$$

be the function spaces we work with here; and for later purposes we also need $W := H^1(B)$. The Euler-Lagrange system for pressurized phase-field fracture reads [57]:

Formulation 1. Let $p \in L^\infty(B)$ be given. Find vector-valued displacements and a scalar-valued phase-field variable $\{u^n, \varphi^n\} := \{u, \varphi\} \in \{u_D + V\} \times W$ such that at each incremental step $n = 1, 2, 3, \ldots$, we solve

$$\left(\left((1 - \kappa)\varphi^2 + \kappa \right) \sigma^+(u), e(w) \right) + (\sigma^-(u), e(w))$$
$$+ (\varphi^2 p, \operatorname{div} w) = 0 \quad \forall w \in V, \tag{3}$$

and

$$(1 - \kappa)(\varphi \, \sigma^+(u) : e(u), \psi - \varphi) + 2(\varphi \, p \operatorname{div} u, \psi - \varphi)$$
$$+ G_c \left(-\frac{1}{\varepsilon}(1 - \varphi, \psi - \varphi) + \varepsilon(\nabla\varphi, \nabla(\psi - \varphi)) \right) \geq 0 \quad \forall \psi \in W_{in} \cap L^\infty(B). \tag{4}$$

Here, G_c is the critical energy release rate, and we use the well-known law for the linear stress-strain relationship:

$$\sigma := \sigma(u) = 2\mu_s e(u) + \lambda_s \operatorname{tre}(u)I, \tag{5}$$

where μ_s and λ_s denote the Lamé coefficients, $e(u) = \frac{1}{2}(\nabla u + \nabla u^T)$ is the linearized strain tensor and I is the identity matrix.

4

Furthermore in 2D, the stress σ is split into tensile σ^+ and compressive parts σ^- [50]:

$$\sigma^+ = 2\mu_s e^+ + \lambda_s < \text{tr}(e) > I,$$
$$\sigma^- = 2\mu_s(e - e^+) + \lambda_s\Big(\text{tr}(e) - < \text{tr}(e) >\Big)I,$$

and

$$e^+ = P\Lambda^+ P^T,$$

where $< \cdot >$ is the positive part of a function. Moreover, for $d = 2$, we have

$$\Lambda^+ := \Lambda^+(u) := \begin{pmatrix} < \lambda_1(u) > & 0 \\ 0 & < \lambda_2(u) > \end{pmatrix},$$

where $\lambda_1(u)$ and $\lambda_2(u)$ are the eigenvalues of the strain tensor e, and $v_1(u)$ and $v_2(u)$ the corresponding (normalized) eigenvectors. Finally, the matrix P is defined as $P := P(u) := (v_1, v_2)$; namely, it consists of the column vectors $v_i, i = 1, 2$. In the 3D examples we simply work in this paper with (5) because only tensile forces will occur in this specific test. Otherwise, we would have utilized the law proposed in [7] as we already implemented in our sister code [43]. A discussion of various splitting laws can be found in [12][Section 2.2] and [3].

Remark 2.1 (Nonlinearities). Formulation 1 is nonlinear due to the monolithic formulation, the term $(1 - \kappa)(\varphi\, \sigma^+(u) : e(u), \psi - \varphi)$, the stress splitting, and the inequality constraint. The most critical term is the quasi-linearity $\Big(\big((1 - \kappa)\varphi^2 + \kappa\big)\, \sigma^+(u), e(w)\Big)$, which causes most of the challenges in designing reliable and efficient solution algorithms. In fact, integrating this term with respect to u yields the corresponding term on the energy level:

$$\Big(\big((1 - \kappa)\varphi^2 + \kappa\big)\, \sigma^+(u), e(u)\Big),$$

which has been well-characterized to be non-convex in both variables u and φ simultaneously in the very early work [14, 13] (there yet without the stress-splitting though). For a simplified computational analysis, we also refer the reader to Section 4 in this paper.

Remark 2.2 (Non-smoothness in time). As it is usual in quasi-static problems, we cannot have any regularity in time. In practice, this means that crack propagation may not be smooth and the solution can have jumps in time in two subsequent loading steps. Specific explanations and justifications for variational phase-field fracture can be found in [13][Section 1.1] and [15]. For similar arguments for the pressurized phase-field fracture model, we refer to [57].

Remark 2.3. In Formulation 1, κ is a (small) positive regularization parameter for the elastic energy. Physically, κ represents the residual stiffness of the material. Consequently, since

$$\Big((1 - \kappa)\varphi^2 + \kappa\Big) \to \kappa \quad \text{for } \varphi \to 0,$$

the material stiffness decreases while approaching the fracture zone.

Remark 2.4. The pressure terms $(\varphi^2 p, \text{div } w)$ and $2(\varphi\, p\, \text{div } u, \psi - \varphi)$ have been derived in [54, 57] and are based on an interface law that has been further manipulated using Gauss' divergence theorem.

Remark 2.5. Formulation 1 does not explicitly contain time-derivatives. Rather, the time t might enter through time-dependent boundary conditions, e.g., $u_D = u_D(t) = g(t)$ on ∂B with a prescribed boundary function $g(t)$ of Dirichlet-type or through time-dependent right hand side forces, e.g., a time-dependent pressure force $p := p(t)$.

2.3. A fully monolithic semi-linear form

For the solution process, we add both equations in Formulation 1 and define a common semi-linear form:

Formulation 2. At each incremental step n, find $U^n := U := \{u, \varphi\} \in \{u_D + V\} \times W$ such that

$$
\begin{aligned}
A(U)(\Psi - U) = & \left(\left((1 - \kappa)\varphi^2 + \kappa \right) \sigma^+(u), e(w) \right) + (\sigma^-(u), e(w)) + (\varphi^2 p, \nabla \cdot w) \\
& + (1 - \kappa)(\varphi\, \sigma^+(u) : e(u), \psi - \varphi) + 2(\varphi\, p\, \nabla \cdot u, \psi - \varphi) \\
& + G_c \left(-\frac{1}{\varepsilon}(1 - \varphi, \psi - \varphi) + \varepsilon(\nabla\varphi, \nabla\psi - \nabla\varphi) \right) \\
\geq & \; 0,
\end{aligned}
\tag{6}
$$

for all $\Psi := \{w, \psi\} \in V \times W_{in}$.

In order to deal with the variational inequality, the constraint $\varphi \leq \varphi^{old}$ is relaxed through penalization as it will be explained in Section 2.4.

2.4. An incremental formulation using augmented Lagrangian penalization

Our strategy is as follows: we first discretize in time and work with the resulting incremental formulation. As already used in the definition of the space W_{in}, the irreversibility constraint (2) is discretized with a backward difference quotient such that

$$
\frac{\varphi - \varphi^{n-1}}{\delta t} \leq 0,
$$

where $\delta t = t^n - t^{n-1}$. Here, $\varphi^{n-1} := \varphi(t^{n-1})$ denotes the previous time step solution and $\varphi := \varphi^n := \varphi(t^n)$ the current solution. An augmented Lagrangian formulation[3] of the irreversibility constraint reads [68]:

$$
\varphi \leq \varphi^{n-1} \quad \rightarrow \quad \min(0, \Xi + \gamma\varphi) + \left[\Xi + \gamma(\varphi - \varphi^{n-1}) \right]^+,
$$

where $\Xi \in L^2$ and $\gamma > 0$ and $[x]^+ := max(x, 0)$. In practice, Ξ will be obtained by an iteration.

Remark 2.6. Simplified implementations of the penalization strategy are

$$
\left[\Xi + \gamma(\varphi - \varphi^{n-1}) \right]^+,
$$

or

$$
\left[\gamma(\varphi - \varphi^{n-1}) \right]^+.
$$

In the latter one, Ξ is not necessary and one saves the additional iteration loop. However, this method is well-known to be less robust because of ill-conditioning of the Jacobian matrix [61].

The resulting formulation then reads:

Formulation 3. Given an initial phase-field $\varphi := \varphi^0$ and given either (time-dependent / time-like-dependent) non-homogeneous boundary data u_D or a pressure $p(t) \neq 0$. Compute for $n = 1, 2, 3, \ldots, N$ the incremental solution $U^n := U = \{u, \varphi\} \in \{u_D + V\} \times W$ such that

$$
A(U)(\Psi) := \overline{A}(U)(\Psi) + ([\Xi + \gamma(\varphi - \varphi^{n-1})]^+, \psi) = 0 \quad \forall \Psi \in V \times W,
$$

where

$$
\begin{aligned}
\overline{A}(U)(\Psi) = & \left(\left((1 - \kappa)\varphi^2 + \kappa \right) \sigma^+(u), e(w) \right) + (\sigma^-(u), e(w)) + (\varphi^2 p, \nabla \cdot w) \\
& + (1 - \kappa)(\varphi\, \sigma^+(u) : e(u), \psi) + 2(\varphi\, p\, \nabla \cdot u, \psi) \\
& + G_c \left(-\frac{1}{\varepsilon}(1 - \varphi, \psi) + \varepsilon(\nabla\varphi, \nabla\psi) \right).
\end{aligned}
\tag{7}
$$

---

[3]For the general idea of the augmented Lagrangian method, we refer the reader to [25, 28].

Remark 2.7 (Imposing the inequality constraint). In order to determine Ξ, we design an adaptive augmented Lagrangian formulation (the outer loop) in which we iterate according to the algorithm presented in [73] (based on [68]). Therein, we have also shown that the adaptive choice of the inner tolerance (namely for Newton's method) can significantly reduce the computational cost.

2.5. Spatial discretization

We finally discuss spatial discretization, which is based on a Galerkin finite element scheme, introducing H^1 conforming discrete spaces $V_h \subset V$ and $W_h \subset W$ consisting of bilinear functions Q_1^c on quadrilaterals (see e.g., [21]). The discretization parameter is denoted by h. The discretized version of Formulation 3 reads:

Formulation 4. Given an initial phase-field $\varphi_h := \varphi_h^0$ and given either (time-dependent / time-like-dependent) non-homogeneous boundary data u_D^h or a pressure $p(t) \neq 0$. Compute for $n = 1, 2, 3, \ldots, N$ the incremental solution $U^n := U_h = \{u_h, \varphi_h\} \in \{u_D^h + V_h\} \times W_h$ such that

$$A(U_h)(\Psi_h) := \overline{A}(U_h)(\Psi_h) + ([\Xi_h + \gamma(\varphi_h - \varphi_h^{n-1})]^+, \psi_h) = 0 \quad \forall \Psi_h \in V_h \times W_h.$$

3. A residual-based modified Newton method with Jacobian modification

Our goal in this section is to develop Newton solvers for treating Formulation 4 in a monolithic fashion. As mentioned in the introduction, detailed studies for brittle fracture are presented in [67, 27, 73]. These approaches work well for standard benchmarks which others also have considered (not necessarily using monolithic approaches [50, 53, 15, 48]), but exhibit difficulties for certain configurations with extremely fast crack growth.

We suggest in the following another method that is inspired from two sources. First, a successfully-used algorithm for nonlinear flow problems is a modified Newton method with Jacobian modification [36, 45, 47]. This raises the question how such a modification can be achieved in phase-field fracture. A hint can be found in [32] in which one block in the Jacobian was zero due to an extrapolation in the phase-field variable, yielding an extremely robust and efficient method. The idea is to introduce a control parameter ω for this specific block in a fully monolithic setting.

3.1. The Jacobian matrix

To apply Newton's method for solving $A(U_h)(\Psi_h) = 0$, we first need to compute the derivative of $A(U_h)(\Psi_h)$. We construct the Jacobian[4] by evaluating the directional derivative

$$A'(U)(\delta U, \Psi) := \lim_{s \to 0} \frac{A(U + s\delta U)(\Psi) - A(U)(\Psi)}{s}$$

with $\delta U := \{\delta u, \delta \varphi\} \in V \times W$, which represents later the Newton update. In detail, the Jacobian is given by:

$$\begin{aligned}
A'(U)(\delta U, \Psi) = & \left(2\delta\varphi(1-\kappa)\varphi\sigma^+(u) + \left((1-\kappa)\varphi^2 + \kappa\right)\sigma^+(\delta u), e(w) \right) + (\sigma^-(\delta u), e(w)) + 2(\delta\varphi\,\varphi p, \operatorname{div} w) \\
& + (1-\kappa)\left(\delta\varphi\sigma^+(u) : e(u) + 2\varphi\,\sigma^+(\delta u) : e(u), \psi\right) + 2p(\delta\varphi\nabla \cdot u + \varphi\,\nabla \cdot \delta u, \psi) \\
& + G_c\left(\frac{1}{\varepsilon}(\delta\varphi, \psi) + \varepsilon(\nabla\delta\varphi, \nabla\psi)\right) \\
& + \gamma(\delta\varphi, \psi)_{A(\varphi)} \quad \forall \Psi := \{w, \psi\} \in V \times W,
\end{aligned} \tag{8}$$

where

$$\mathcal{A}(\varphi) = \{x = (x_1, x_2, x_3) \in B \mid \Xi + \gamma\left(\varphi(x) - \varphi(x)^{n-1}\right) > 0\}.$$

In $\sigma^+(\delta u)$ and $\sigma^-(\delta u)$ we employ the derivative of e^+, which is given by

$$e^+(\delta u) = P(\delta u)\Lambda^+ P^T + P\Lambda^+(\delta u)P^T + P\Lambda^+ P^T(\delta u).$$

---

[4]In this section, we omit the index h to simplify the notation.

Remark 3.1 (on the critical term). Recalling Remark 2.1, we observe that the critical term in the matrix is contained in

$$\Big(2\delta\varphi(1-\kappa)\varphi\sigma^+(u) + \big((1-\kappa)\varphi^2 + \kappa\big)\,\sigma^+(\delta u), e(w)\Big). \tag{9}$$

Consulting our computational experiences from [32, 73] in which we designed a very efficient and robust method by neglecting the cross-term block, we conjecture that the most critical term is the off-diagonal contribution

$$2\delta\varphi(1-\kappa)\varphi\sigma^+(u).$$

Related observations have been made in related studies on yield stress fluids (see [45]), where usually the derivative of the nonlinear factor causes most difficulties in the solution process. Indeed in Section 4, we provide a detailed simplified analysis showing that the cross-term significantly determines the properties of the Jacobian matrix.

3.2. Residual-based Newton's method with line-search and quasi-Newton steps

In this section, we first recapitulate a monotonicity-based Newton algorithm. Globalization[5] may be achieved by a damping strategy based on a backtracking line search algorithm. After having presented the algorithm, we explain the steps to change to a modified Newton scheme with Jacobian modification.

To measure the residuals and monitoring functions, we use the discrete norm $\|\cdot\| := \|\cdot\|_{l^2}$. At a given time instance t^n, we shall find the time step solution U^n using:

Algorithm 3.1 (Residual-based Newton's method). In this type of methods, the main criterion is a decrease of the residual in each step. Choose an initial Newton guess U^0. For the iteration steps $k = 0, 1, 2, 3, \ldots$:

1. Find $\delta U^k := \{\delta u, \delta\varphi\} \in V \times W$ such that

$$A'(U^k)(\delta U^k, \Psi) = -A(U^k)(\Psi) \quad \forall \Psi \in V \times W, \tag{10}$$
$$U^{k+1} = U^k + \lambda_k \delta U^k, \tag{11}$$

   for $\lambda_k = 1$.

2. The criterion for convergence is the contraction of the residuals:

$$\|A(U^{k+1})(\Psi)\| < \|A(U^k)(\Psi)\|. \tag{12}$$

3. If (12) is violated, re-compute in (11) U^{k+1} by choosing $\lambda_k^l = 0.5$, and compute for $l = 1, ..., l_M$ (e.g. $l_M = 5$) a new solution

$$U^{k+1} = U^k + \lambda_k^l \delta U^k$$

   until (12) is fulfilled for a $l^* < l_M$ or l_M is reached. In the latter case, no convergence is obtained and the program aborts.

4. In case of $l^* < l_M$ we check next the stopping criterion:

$$\|A(U^{k+1})(\Psi)\| \leq TOL_N.$$

   If this is criterion is fulfilled, set $U^n := U^{k+1}$. Else, we increment $k \to k+1$ and goto Step 1.

Remark 3.2 (Changes in the modified Newton scheme). In the modified Newton scheme that we present below in more detail, we shall work with a modified Jacobian $A'_\omega(U^k)(\delta U^k, \Psi)$ and no line search, i.e., $\lambda_k = 1$ for all k. Furthermore, Step 2 (inequality 12) is omitted. In place of Step 3, we compute heuristically a control parameter ω, which is derived in Section 3.5.

---

[5]The terminology 'globalization' is adopted from numerical optimization (e.g., [61]) or, in general, Newton methods (e.g., [22]) and means that the convergence radius of Newton's method is extended by, for example, line search or trust region methods.

Remark 3.3 (On using quasi-Newton steps). Usually, when the Newton reduction rate

$$\theta_k = \frac{\|A(U^{k+1})(\Psi)\|}{\|A(U^k)(\Psi)\|},$$

was sufficiently good, e.g., $\theta_k \leq \theta_{max} < 1$ (where e.g. $\theta_{max} \approx 0.1$), a common strategy is to work with the 'old' Jacobian matrix, but with a new right hand side. This procedure is well established in the literature (see e.g., [22]) and works usually very well. In phase-field fracture, we found the contrary that the matrix $A'(U^k)(\delta U^k, \Psi)$ should be assembled at each Newton iteration step k such that it fits as well as possible to the corresponding right hand side $A(U^k)(\Psi)$. This is reasonable from a theoretical point of view since the matrix is indefinite and the problem non-convex. Thus, smallest perturbations between matrix and right hand side, may lead to large mismatches, which then further result in a blow-up of the residual and therefore divergence of Newton's method causing the iteration to stop. In Section 5, we illustrate our experiences with the help of one example.

3.3. A Newton method with line-search based on energy monitoring

In this section, we implement another line-search based Newton method while monitoring the global energy. This idea has been applied to phase-field fracture in [27]. Furthermore, as it is well-known in numerical optimization for highly non-convex problems [61], the authors of [27] implemented a strategy that also allows for negative curvatures of the Newton path by utilizing negative line search parameters λ_k.

The key idea relies on the energy representation of the underlying Formulation 1. For quasi-static brittle fracture in elasticity this is the original functional proposed and analyzed in [14, 15]. For pressurized fractures, the corresponding energy functional has been designed and analyzed in [54]. The latter one reads:

$$E(u,\varphi) = \frac{1}{2}\int_B \left((1-\kappa)\varphi^2 + \kappa\right)\sigma(u):e(u)\,dx + \int_B \varphi^2 p\nabla\cdot u\,dx + G_c\int_B\left(\frac{1}{2\varepsilon}(1-\varphi)^2 + \frac{\varepsilon}{2}|\nabla\varphi|^2\right)dx. \tag{13}$$

When we formally extend this functional utilizing stress-splitting and explicitely account for the crack irreversibility constraint, we arrive at:

$$E(U) := E(u,\varphi) = \frac{1}{2}\int_B \left((1-\kappa)\varphi^2 + \kappa\right)\sigma^+(u):e(u)\,dx + \int_B \sigma^-(u):e(u)\,dx + \int_B \varphi^2 p\nabla\cdot u\,dx$$
$$+ G_c\int_B\left(\frac{1}{2\varepsilon}(1-\varphi)^2 + \frac{\varepsilon}{2}|\nabla\varphi|^2\right)dx + I_{K(\varphi^{n-1})}(\varphi), \tag{14}$$

where $I_{K(\varphi^{n-1})}(\varphi)$ is the energy form of the penalization term of one of the possible strategies given in Section 2.4. For details, we refer the reader to [68][Section 3]. A formal differentiation of $E(u,\varphi)$ with respect to u and φ into the directions w and ψ yields

$$E'(U)(\Psi) := E'(u,\varphi;w,\psi) = A(u,\varphi)(w,\psi) =: A(U)(\Psi)$$

and thus Formulation (3).

We are now prepared for stating the algorithm. In our notation, a slightly-adapted algorithm proposed in [27] reads:

Algorithm 3.2 (A Newton method with line-search based on energy monitoring). The main criterion is a decrease of the energy $E(U)$ at each step. Choose an initial Newton guess U^0. For the iteration steps $k = 0, 1, 2, 3, \ldots$:

1. Find $\delta U^k := \{\delta u, \delta \varphi\} \in V \times W$ such that

$$A'(U^k)(\delta U^k, \Psi) = -A(U^k)(\Psi) \quad \forall \Psi \in V \times W, \tag{15}$$

$$U^{k+1} = U^k + \lambda_k \delta U^k, \tag{16}$$

for $\lambda_k = 1$.

2. The criterion for convergence is the decrease of energy:

$$E(U^{k+1}) < E(U^k) + R, \tag{17}$$

where $R > 0$ is a number to allow for a slight increase of the energy due to numerical errors (round-off, for instance). In our numerical tests, we choose a rather large value $R = 0.01$, which avoids going to often into the line search loop and still yields the reliable numerical results.

3. If (17) is violated, re-compute in (16) U^{k+1} by choosing $\lambda_k^l \in [-1, 1]$ and update accordingly

$$U^{k+1} = U^k + \lambda_k^l \delta U^k,$$

until (17) is fulfilled. How to obtain λ_k^l is explained in Remark 3.4.

4. We check next the stopping criterion:

$$\|A(U^{k+1})(\Psi)\| \leq TOL_N.$$

If this is criterion is fulfilled, set $U^n := U^{k+1}$ and goto the next loading step. Else, we increment $k \to k + 1$ and goto Step 1 in this Newton algorithm.

Remark 3.4 (on negative line search parameters). A standard line search algorithm tries to find $\lambda_k^l \in (0, 1]$ in Step 3. If a negative curvature is detected at $\lambda_k^l = 0$ (for details we refer to [27][Section 4.2]), it might be necessary to allow for negative λ_k^l. One possible choice is to extend the line-search parameter interval to $[-1, 0)$. Our version is to discretize the interval $[-1, 1]$ by taking uniform step sizes λ_k^l, e.g., $l = 40$, and to check condition (17) in Step 3 of the above algorithm. The first 20 line search steps are taken from $(0, 1]$. If they do not yield a satisfactory energy decrease, we choose 20 negative values from less than 0 to -1. An accurate method to choose an optimal λ_k^l is described in [27][Section 4.2.1]. When necessary, we bypass these additional computations and simply take a larger l to satisfy condition (17).

Remark 3.5. The authors of [27] also observed sometimes an energy increase, which is not possible with the above algorithm. Indeed, the line-search procedure in [27] was only activated after certain 'critical' situations (e.g., a sharp energy increase) were observed.

Remark 3.6. Another, somewhat similar, adaptation would be to use

$$E(U^{k+1}) < E(U^0) + R, \tag{18}$$

rather than (17). The most important aspect is a final energy decrease in comparison to the initial energy $E(U^0)$. Thus, this idea allows intermediate violations of (17) and thus a relaxation of the very strict monitor.

Remark 3.7 (Limitations of the energy-based line-search monitor). Monitoring the energy in Newton's method is simple for the equations considered in this paper. However, we emphasize that this idea is limited to problems that allow for an energy formulation. For instance, the extension to a fully monolithic fluid-filled fracture formulation does not yield a global energy functional, but only a free energy (Lyapunov) functional with dissipation as explained in [56][Section 2.4]. On the other hand, using splitting algorithms that decouple other physics from the phase-field displacement system [44] would still allow to implement an energy monitor in the time-discretized (i.e., incremental) version of the problem.

3.4. Block structure of the Jacobian, solution vector, and right hand side

Before we can design another Newton method, we need to understand the structure of the linear system (10) to be solved at each Newton iteration. For the spatial discretization, we use the previously introduced spaces $V_h \times W_h$ with vector-valued basis

$$\{\psi_i \,|\, i = 1, \ldots, N\},$$

where the basis functions are primitive (they are only non-zero in one component), so we can separate them into displacement and phase-field basis functions and sort them accordingly:

$$\psi_i = \begin{pmatrix} \chi_i^u \\ 0 \end{pmatrix}, \text{ for } i = 1, \ldots, N_u,$$

$$\psi_{(N_u+i)} = \begin{pmatrix} 0 \\ \chi_i^\varphi \end{pmatrix}, \text{ for } i = 1, \ldots, N_\varphi,$$

where $N_u + N_\varphi = N$. This is now used to transform (10) into a system of the form

$$M\delta U = F, \tag{19}$$

where M is a block matrix (the Jacobian) and F the right hand side consisting of the residuals. The unknown solution vector is δU. The block structures are

$$M = \begin{pmatrix} M^{uu} & M^{u\varphi} \\ M^{\varphi u} & M^{\varphi\varphi} \end{pmatrix}, \qquad F = \begin{pmatrix} F^u \\ F^\varphi \end{pmatrix}, \qquad \delta U = \begin{pmatrix} \delta U^u \\ \delta U^\varphi \end{pmatrix},$$

with entries coming from (8):

$$M_{i,j}^{uu} = \left(\left((1-\kappa)\varphi^2 + \kappa\right)\sigma^+(\chi_j^u), e(\chi_i^u)\right) + (\sigma^-(\chi_j^u), e(\chi_i^u)),$$

$$M_{i,j}^{u\varphi} = \left(2\chi_j^\varphi(1-\kappa)\varphi\sigma^+(u), e(\chi_i^u)\right) + 2\,(\chi_j^\varphi \varphi p, \operatorname{div}\chi_i^u),$$

$$M_{i,j}^{\varphi u} = 2(1-\kappa)(\varphi\,\sigma^+(\chi_j^u) : e(u), \chi_i^\varphi) + 2p(\varphi\operatorname{div}(\chi_j^u), \chi_i^\varphi),$$

$$M_{i,j}^{\varphi\varphi} = (1-\kappa)(\sigma^+(u) : e(u)\chi_j^\varphi, \chi_i^\varphi) + 2p(\operatorname{div}(u)\chi_j^\varphi, \chi_i^\varphi)$$
$$\qquad + G_c\left(\frac{1}{\varepsilon}(\chi_j^\varphi, \chi_i^\varphi) + \varepsilon(\nabla\chi_j^\varphi, \nabla\chi_i^\varphi)\right) + \gamma(\chi_j^\varphi, \chi_i^\varphi)_{A(\varphi)}.$$

The right hand side consists of the corresponding residuals (see Formulation 3 and therein (7)). In particular, we have

$$F_i^u = -A(U^k)(\chi_i^u)$$
$$= \left(\left((1-\kappa)\varphi_k^2 + \kappa\right)\sigma^+(u_k), e(\chi_i^u)\right) + (\sigma^-(u_k), e(\chi_i^u)) + (\varphi_k^2 p, \operatorname{div}\chi_i^u),$$

$$F_i^\varphi = -A(U^k)(\chi_i^\varphi) = (1-\kappa)(\varphi_k\,\sigma^+(u_k) : e(u_k), \chi_i^\varphi) + 2(\varphi_k\, p \operatorname{div} u_k, \chi_i^\varphi)$$
$$\qquad + G_c\left(-\frac{1}{\varepsilon}(1-\varphi_k, \chi_i^\varphi) + \varepsilon(\nabla\varphi_k, \nabla\chi_i^\varphi)\right) + ([\Xi_h + \gamma(\varphi_k - \varphi_k^{n-1})]^+, \chi_i^\varphi).$$

In the matrix, the degrees of freedom that belong to Dirichlet conditions (here only the displacements since we assume Neumann conditions for the phase-field variable) are strongly enforced by replacing the corresponding rows and columns as usually done in a finite element code.

3.5. A modified Newton method with Jacobian modification

Rather than employing line search in Step 3 in Algorithm 3.1, we introduce a control parameter $\omega \in [0, 1]$ inside the Jacobian, which decides whether a full Newton system ($\omega = 1$), a Newton-like system with $0 < \omega < 1$ or even $\omega = 0$ is solved. The choice of this parameter is heuristic, but the key idea very simple. Inspired by several studies that have been performed for nonlinear flow [36, 45, 47], we further develop these concepts in the following.

As shown in Section 3.4, formally, the Jacobian reads at each Newton step k:

$$M = \begin{pmatrix} M^{uu} & M^{u\varphi} \\ M^{\varphi u} & M^{\varphi\varphi} \end{pmatrix}.$$

The critical block is $M^{u\varphi}$, particularly

$$(2\chi_j^\varphi (1-\kappa)\varphi\sigma^+(u), e(\chi_i^u)) \tag{20}$$

as it was already identified in [32] (see also the Remarks 3.8 below and 3.1 above). Thus the goal is to design a procedure in which this block is dynamically activated or disabled during a Newton iteration. Incorporating ω brings us to

$$M = \begin{pmatrix} M^{uu} & \omega M^{u\varphi} \\ M^{\varphi u} & M^{\varphi\varphi} \end{pmatrix} = \begin{pmatrix} M^{uu} & 0 \\ M^{\varphi u} & M^{\varphi\varphi} \end{pmatrix} + \omega \begin{pmatrix} 0 & M^{u\varphi} \\ 0 & 0 \end{pmatrix}. \tag{21}$$

Remark 3.8 (Extrapolated scheme). In the extrapolated scheme, we replace φ^2 by a linear-in-time extrapolation $\tilde\varphi^2$ in the first line of the residual (7). When computing the Jacobian, the block $M_{i,j}^{u\varphi}$ is zero after differentiation with respect to φ. Therefore, the matrix M has always a triangular block structure:

$$M = \begin{pmatrix} M^{uu} & 0 \\ M^{\varphi u} & M^{\varphi\varphi} \end{pmatrix}. \tag{22}$$

This pattern greatly facilitates the linear solution, particularly the design of preconditioners when using an iterative technique, such as GMRES, for instance. Evidence is shown in several studies for 2D and 3D problems where we could extend relatively easily the idea presented in [32] to parallel computations in 3D [43].

Remark 3.9. Since the blocks $M^{\varphi u}$ and $M^{u\varphi}$ are identical since the matrix M is symmetric by construction, one may try to build a symmetric approximation by

$$M = \begin{pmatrix} M^{uu} & \omega M^{u\varphi} \\ \omega M^{\varphi u} & M^{\varphi\varphi} \end{pmatrix} = \begin{pmatrix} M^{uu} & 0 \\ 0 & M^{\varphi\varphi} \end{pmatrix} + \omega \begin{pmatrix} 0 & M^{u\varphi} \\ M^{\varphi u} & 0 \end{pmatrix}. \tag{23}$$

We carried out some further numerical tests exploiting this idea (not shown in this paper though), but found inferior performance of the Newton solver. From a numerical standpoint, this is clear because removing more terms in the matrix weakens further the performance of the Newton scheme since the Jacobian and the residual fit less together. For this reason, we did not further pursue this idea in our current work and we worked rather with the decomposition (21).

3.5.1. Computing the control parameter ω

The choice of ω is done in a dynamic way dependent on the previous two Newton residuals. Thus, at each Newton step k, the parameter $\omega := \omega_k$ is updated if applicable.

We define the residual and reciprocal residual reductions, respectively:

$$Q_{k+1} = \frac{\|A(U^{k+1})(\Psi)\|}{\|A(U^k)(\Psi)\|}, \quad Q_{k+1}^{rec} = \frac{\|A(U^k)(\Psi)\|}{\|A(U^{k+1})(\Psi)\|}. \tag{24}$$

If $Q_{k+1} < 1$, the new residual is smaller and we classify this step as a 'good' step. Moreover, if $Q_{k+1} \to 0$, the better the current step. On the other hand, if $Q_{k+1} \geq 1$, the new residual is larger than the old one and we have the situation in which a monotonicity-based Newton method would fail and, for example, an error-oriented version may perform better [22].

We summarize the key ideas and construction of the control parameter ω in the following:

Definition 3.3 (Computing ω_{k+1}). At the Newton step k, let $0 \leq \omega_k \leq 1$ be given and let $S \in \mathbb{R}_+ \cup \{0\}$. We define

$$\omega := \omega_{k+1} = S\omega_k. \tag{25}$$

Proposition 3.4 (Motivation of S)**.** The scaling parameter S is motivated as follows:

1. S must yield $\omega_{k+1} \in [0, 1]$.
2. $S \gg 1$ should yield $\omega_{k+1} \to 1$ (full Newton).
3. $S \to 0$ should yield $\omega_{k+1} \to 0$ (Newton-like / fixed-point like scheme).

Proposition 3.5 (A specific realization of S)**.** Given Proposition 3.4, the scaling parameter S can be realized, using the residuals Q_{k+1} and Q_{k+1}^{rec} defined in (24), as follows:

1. For $Q_{k+1} \to 0$ (and $Q_{k+1}^{rec} \to \infty$) the matrix M defined in (21) has good properties and we can work with a full Newton step, i.e., $S \gg 1$ yielding $\omega_{k+1} = 1$.
2. On the other hand, for $Q_{k+1}^{rec} \to 0$ (and $Q_{k+1} \to \infty$), the matrix M becomes ill-conditioned, and $S \to 0$ yielding $\omega_{k+1} \ll 1$ should be employed.
3. These observations yield the following possible realization of S:

$$S := \left(\frac{a}{\exp(Q_{k+1}^{rec})} + \frac{b}{\exp(Q_{k+1})} \right). \tag{26}$$

4. The control parameter a is related to a fixed-point step with small ω_{k+1} and thus $a < 1$ should be chosen.
5. The control parameter b is related to a full Newton step with $\omega_{k+1} = 1$ and thus $b \geq 1$ should be chosen.
6. Both control parameters will be further explained and specified in Section 3.5.3.

Corollary 3.6 (Further properties of S)**.** The scaling parameter S has the following properties:

1. S is bounded from below by zero: since $a, b, Q_{k+1}, Q_{k+1}^{rec} \geq 0$, we have $S \geq 0$ yielding $\omega_{k+1} \geq 0$.
2. S is not bounded from above. Consequently, it may easily happen that $\omega_{k+1} > 1$ in (25). Therefore we use a simple projection:
$$\text{Set} \quad \omega_{k+1} := 1 \quad \text{if} \quad \omega_{k+1} > 1.$$

3.5.2. The modified Newton algorithm

We define

$$
\begin{aligned}
A'_\omega(U)(\delta U, \Psi) = & \Big(\omega 2\delta\varphi(1-\kappa)\varphi\sigma^+(u) + \big((1-\kappa)\varphi^2 + \kappa\big) \sigma^+(\delta u), e(w) \Big) + (\sigma^-(\delta u), e(w)) + 2\,(\omega\delta\varphi\,\varphi p, \operatorname{div} w) \\
& + (1-\kappa)\Big(\delta\varphi\sigma^+(u) : e(u) + 2\varphi\,\sigma^+(\delta u) : e(u), \psi \Big) + 2p(\delta\varphi\nabla \cdot u + \varphi\,\nabla \cdot \delta u, \psi) \\
& + G_c\Big(\frac{1}{\varepsilon}(\delta\varphi, \psi) + \varepsilon(\nabla\delta\varphi, \nabla\psi) \Big) \\
& + \gamma(\delta\varphi, \psi)_{A(\varphi)} \quad \forall\Psi := \{w, \psi\} \in V \times W,
\end{aligned}
\tag{27}
$$

which is (8) except that the terms with $\delta\varphi$ multiplied by the w test function are scaled with ω and in particular the very first term.

At a given time instance t^n, we shall find the time step solution U^n using:

Algorithm 3.7 (Modified Newton's method with Jacobian modification)**.** Choose an initial Newton guess U^0 and an initial guess for the control parameter, i.e., $\omega_0 = 1$. For the iteration steps $k = 0, 1, 2, 3, \ldots$:

1. Find $\delta U^k := \{\delta u, \delta\varphi\} \in V \times W$ such that

$$A'_\omega(U^k)(\delta U^k, \Psi) = -A(U^k)(\Psi) \quad \forall\Psi \in V \times W, \tag{28}$$

$$U^{k+1} = U^k + \delta U^k. \tag{29}$$

2. Compute:

$$\omega := \omega_{k+1} = S\,\omega_k, \tag{30}$$

with S determined by (26).

13

3. Check

$$\|A(U^{k+1})(\Psi)\| \leq TOL_N.$$

If this criterion is fulfilled, set $U^n := U^{k+1}$. Else, we increment $k \to k + 1$ and goto Step 1.

Remark 3.10. In this algorithm, we do not have any convergence monitor and it can happen that Newton's method diverges. Thus, we also check in Step 3 whether

$$\|A(U^{k+1})(\Psi)\| < TOL_N^{up}, \quad TOL_N^{up} = 10^{12},$$

otherwise we stop the algorithm because of divergence. In Section 5, we see that for backtracking line-search such a behavior is indeed detected, but in which the modified Newton method (without convergence monitor) yields excellent performance. We notice that TOL_N^{up} seems very high, but there are examples in Section 5 where the residual goes up to 10^7 but nonetheless Newton's method will finally still converge.

3.5.3. On the choice of a and b

The choices of a and b are heuristic. As outlined in Proposition 3.5, the parameter a controls the influence of block $M^{u\varphi}$. The parameter b controls the rate to go back to full Newton steps in case sufficient performance of the solver is detected. Therefore, we propose the following bounds:

$$0 \leq a < 1 \quad \text{and} \quad 1 \leq b < \infty.$$

Let us discuss the idea in more detail. If $Q_{k+1} \ll 1$ we had a good reduction and we can use a higher ω_{k+1} in the next step. Formula (26) yields

$$\lim_{Q_{k+1}^{rec} \to \infty} \lim_{Q_{k+1} \to 0} S \to b \quad \Rightarrow \quad \omega_{k+1} = b\omega_k \quad \Rightarrow \quad \omega_{k+1} \geq \omega_k.$$

On the other hand if $Q_{k+1} > 1$ or even $Q_{k+1} \gg 1$ (thus $Q_{k+1}^{rec} \to 0$) we want to eliminate the irregular terms in the Jacobian matrix and rather work with a Newton-like method in which the Jacobian is approximated by minimizing the influence of the term (20). Here:

$$\lim_{Q_{k+1}^{rec} \to 0} \lim_{Q_{k+1} \to \infty} S \to a \quad \Rightarrow \quad \omega_{k+1} = a\omega_k \quad \Rightarrow \quad \omega_{k+1} < \omega_k.$$

Since due to the construction, we cannot ensure a priori that S is bounded from above, the requirement $0 \leq \omega_{k+1} \leq 1$ may be violated. In this case, a projection is used (see Corollary 3.6).

Possible choices of a and b:

- Choice 1: $a = 0.001$ and $b = 10$ drastically tries to remove the entire block $M^{u\varphi}$ and moderately goes back to full Newton;

- Choice 2: $a = 0.1$ and $b = 2$ tries moderately to remove the influence of block $M^{u\varphi}$ and moderately goes back to full Newton;

- Choice 3: $a = 0$ and $b = 0$ resulting in $S = 0$ from which we obtain $\omega_k = 0$ for all k and thus never work with block $M^{u\varphi}$.

Obviously, the smaller $a \ll 1$ is chosen, the faster we obtain a Newton-like (fixed-point) scheme. Secondly, the larger we choose $b \geq 1$, the faster we go back to a full Newton scheme. For more choices of a and b and their consequences in the numerical examples, we specifically refer to Section 5.1.

4. Computational analysis of a simplified characteristic problem

We illustrate the features of the underlying equations and behavior of Newton's method with a very simple example. This configuration has many characteristic features of the original problem and enables us to study some important properties of Newton's method.

In $\mathbb{R}^2$ we want to minimize the function $F : \mathbb{R}^2 \to \mathbb{R}$ given by

$$F(x, y) = (\kappa + x^2)y^2, \quad \kappa > 0, \quad (x, y) \in \mathbb{R}^2.$$

The function is visualized in Figure 2.

Remark 4.1 (Link to phase-field fracture). In phase-field fracture, the critical part of the underlying energy functional (see e.g., Functional (13)), originally proposed without any pressures and for $\mathbb{C}|e(u)|^2 = |\nabla u|^2$ in [26, 14], is:

$$E_{crit}(u, \varphi) = \frac{1}{2} \int_B \underbrace{(\kappa + (1 - \kappa)\varphi^2)}_{\sim(\kappa + x^2)} \underbrace{\mathbb{C}|e(u)|^2}_{\sim y^2} \, dx, \tag{31}$$

where $\mathbb{C}e(u) = \sigma(u) := 2\mu e(u) + \lambda tr(e(u))I$.

The function $F(x, y)$ represents the main term of the energy formulation of the fracture problem in a simplified fashion. Here the variable x represents φ and y the displacements u (i.e., the stresses $\sigma(u)$). Clearly, we see that the minimal value of $F(x, y)$ is zero, however the solution (x, y) is not unique: any pair $(x, 0)$ with $x \in \mathbb{R}$ will yield $F(x, 0) = 0$. The non-uniqueness is due to the non-convexity of $F(x, y)$.
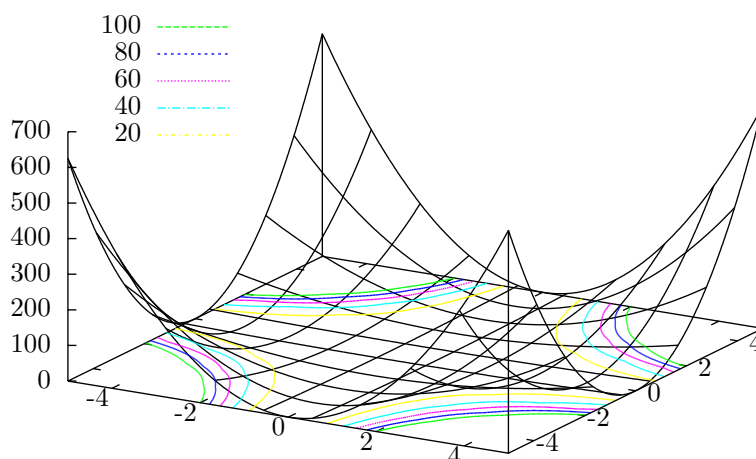
Figure 2: Visualization of $F(x, y)$ and its contour lines. Specifically, we easily see that the minimum is not unique. We also observe that by fixing one variable, the problem becomes strictly convex in the other unknown.

To solve the above problem numerically, we calculate the first-order derivative[6]

$$F'(x, y) = (2xy^2, 2(\kappa + x^2)y)^T.$$

In order to solve $F'(x, y) = 0$ for obtaining the solution pair (x, y), we apply Newton's method. The Hessian[7] of $F(x, y)$ is given by:

$$H_f := H_f(x, y) = F''(x, y) = \begin{pmatrix} 2y^2 & 4xy \\ 4xy & 2(\kappa + x^2) \end{pmatrix}.$$

---

[6]In PDE language, the so-called residual.
[7]In PDE language the so-called Jacobian.

It is obvious to see that H_f is indefinite with the determinant $det(H_f) = -12x^2y^2 + 4\kappa y^2$. Consequently, Newton's method, given (x_0, y_0), find (x_{k+1}, y_{k+1}) for $k = 0, 1, 2, 3, \ldots$,

$$H_f(x_k, y_k)(\delta x, \delta y)^T = -F'(x_k, y_k),$$
$$\begin{pmatrix} x_{k+1} \\ y_{k+1} \end{pmatrix} = \begin{pmatrix} \delta x \\ \delta y \end{pmatrix} + \begin{pmatrix} x_k \\ y_k \end{pmatrix},$$

might produce non-descending steps.

In the following, we carry out some computations with interesting results. The programming code is based on octave [38] and is a further extension of [37]. In the first setting, we take $\kappa = 0.01$ and as initial Newton guess, we take $(x_0, y_0) = (-5, 4)$. The only convergence monitoring criterion is whether the residual norm is smaller than a given tolerance, i.e.,

$$|F'(x_{k+1}, y_{k+1})| < TOL, \quad TOL = 10^{-8}.$$

Despite being close to an optimal solution, Newton's method needs 27 iterations to converge. As optimal solution we obtain

$$\bar{x} = 8.71 \times 10^{-4}, \quad \bar{y} = 2.20 \times 10^{-7}.$$

Here, indeed $F(\bar{x}, \bar{y}) = 4.82 \times 10^{-16} \approx 0$. However the most significant observation is that Newton's method does not converge monotonically but exhibits slight oscillations as visualized in Figure 3. Therefore, any monotonicity-based Newton method would fail.
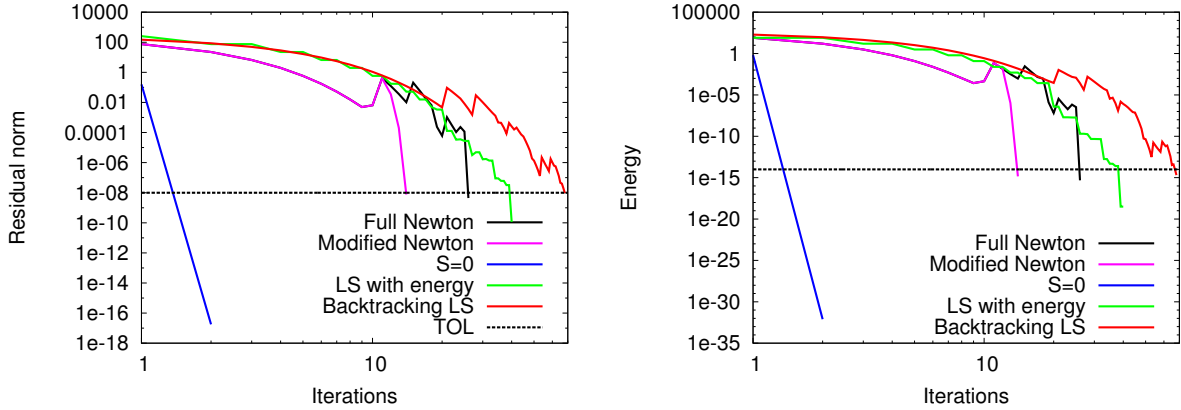
Figure 3: Evolution of the residual norm $|F'(x_k, y_k)|$ (left) and the energy $F(x_k, y_k)$ (right) for full Newton (no modifications), modified Newton ($a = 0.01, b = 5$), Newton with $S = 0$, the line-search procedure with energy monitor (LS with energy), and a backtracking line search with $\lambda_k = 0.5$. Using the line-search procedure with energy monitor, we notice that two times, namely at the Newton steps $k = 23$ and $k = 30$, a negative $\lambda_k = -0.05$ is chosen, which justifies [27] to consider also negative curvatures of the Newton path. The performances of all algorithms in this example depend on the initial guess (x_0, y_0) and the choice of the solver parameters a, b, S, λ_k and R. Therefore, other parameter choices could further reduce the number of Newton iterations, in particular for the last two schemes with line-search procedures.

In our second test, we work with Algorithm 3.7. Introducing ω, the Hessian matrix reads:

$$\begin{pmatrix} 2y^2 & \omega 4xy \\ 4xy & 2(\kappa + x^2) \end{pmatrix}.$$

Choosing $a = 0.01$ and $b = 5$, we obtain the result in 15, much less, iterations:

$$\bar{x} = 2.62 \times 10^{-4}, \quad \bar{y} = 3.79 \times 10^{-7},$$

with $F(\bar{x}, \bar{y}) = 1.44 \times 10^{-15}$.

16
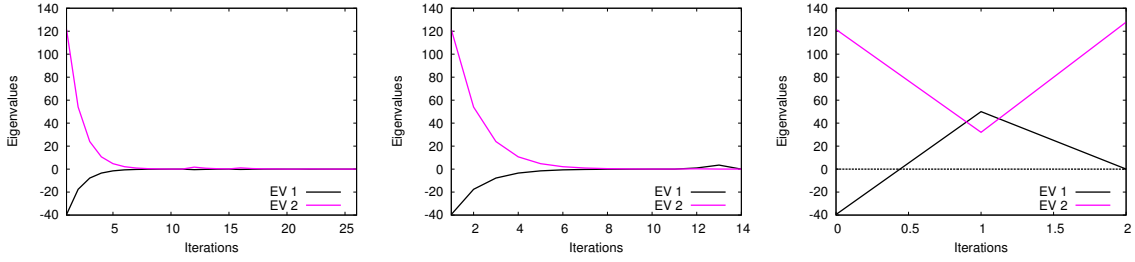
Figure 4: Evolution of the eigenvalues for the three test cases full Newton, modified Newton and $S = 0$.

We also choose the extreme case $S = 0$ resulting in $\omega = 0$, thus

$$H_f(x, y) = \begin{pmatrix} 2y^2 & 0 \\ 4xy & 2(\kappa + x^2) \end{pmatrix}.$$

Here, the matrix H_f becomes positive semi-definite $det(H_f) = 4x^2y^2 + 4\kappa y^2$, even positive definite for any $y \neq 0$. Thus, Newton can converge extremely fast in two steps, despite the fact that the modified H_f does not correspond to the true derivative of the right hand side residual $F'(x, y)$. Indeed, we observe

$$\bar{x} = 0, \quad \bar{y} = -8.88 \times 10^{-16},$$

and $F(\bar{x}, \bar{y}) = 7.89 \times 10^{-33} \approx 0$. The evolution of the eigenvalues that confirm the properties of the respective Hessian matrices are pictured in Figure 4.

We next perform two additional computations using Algorithm 3.1 with $\lambda_k = 0.5$ and Algorithm 3.2 with $R = 0$ and $l = 40$. These findings are also displayed in Figure 3. In particular, the line-search procedure with energy monitoring (Section 3.3) minimizes at each Newton step the global energy $F(x_k, y_k)$. In general the residual norm has the same behavior, but there are steps $k = 24, 28, 31$ in which the energy decreases, but the residual does increase.

Of course, our problem of interest in Section 2 is more complex since we do not seek a single point, but a solution (u^k, φ^k) minimizing $E(u^k, \varphi^k)$ in a function space setting. We cannot expect in general that the Newton-like scheme with $\omega < 1$ converges as fast as in this example. However, these findings indicate us that the modified Newton scheme may work for the original problem at hand.

Recapitulating the key findings of this section, we found that even for a pretended very simple optimization problem, Newton's method does not converge monotonically and may need many iterations. Secondly, the modification of the Jacobian according to Section 3.5 can yield a significant reduction of iteration steps. Thirdly, the line-search method with energy monitoring can specifically control the total energy, but should allow for working with negative line-search parameters.

5. Numerical tests

In this final section, we shall investigate the performance of the modified Newton scheme with Jacobian modification. We study several numerical tests: revisiting a benchmark from mechanics, e.g., [50] in which previously other nonlinear schemes already worked well. Secondly, we compute a propagating pressurized fracture [68] in which previously extremely many iterations were required. Next, a screw tension test is considered [69], which would not work so far for fully monolithic formulations [73]. Finally, we consider two 3D scenarios each with two fractures. In Table 1, we briefly explain the schemes implemented in this paper.

Furthermore, in all tests the inexact augmented Lagrangian iteration from [73] is adopted. Here, the tolerance of the Newton solver is chosen adaptively with respect to the L_2 error of the augmented Lagrangian iteration. All numerical examples in this paper are computed with a self-developed code based on the open-source finite element package deal.II [10, 9] and specifically on the deal.II-template for solving nonlinear coupled PDE-multiphysics problems [70].

17

Table 1: Newton schemes used in this work.

No.	Name used in Sec. 5	Scheme	Features
1	Mod. New	Modified Newton	$a = 0.01, b = 5$; adaptive choice of ω_k
2	Line search New. / LS New.	Newton line search	Backtracking line search with max. 5 LS iterations
3	$S = 0$	Modified Newton	$S = 0$; thus $\omega_k = 0$ for all k
4	Mod. New + Line search (LS)	Mixed Newton	Combining schemes 1 and 2
5	Mod. New. + QN steps	Modified Newton	Jacobian not build at every iteration step
6	No criterion	Newton	no LS, $\omega_k = 1$, no check of Step 3 in Alg. 3.1
7	$a = x, b = y$	Modified Newton	Different values than in 1, e.g., $x = 0.05, y = 2$.
8	LS with Energy	Newton line search	Line search with energy monitor (Section 3.3)

5.1. Single edge notched shear test

In this first example, we restrict our attention to an elastic crack-propagation example. The geometric and material properties are the same as used in [50]. In the single edge notched shear test, it is important to consider the correct boundary conditions and the spectral decomposition of the stress $\sigma(u)$ into tensile $\sigma^+(u)$ and compressive parts $\sigma^-(u)$. We refer to [53, 7] for a detailed physical motivation. A comparison highlighting the properties of one or the other splitting model has been published in [3]. In particular, the Miehe et al. splitting does not release all stresses once the fracture reaches the bottom part of the specimen. The characteristic feature of this test is that an initial crack is prescribed in the geometry rather than with phase-field and that the crack will slowly develop, followed by faster growth.

Configuration. The geometry and boundary conditions are displayed in Figure 5. In particular the initial domain has already a slit (fracture). The initial mesh is 4, 5 and 6 times uniformly refined, leading to $1024, 12771$ and 50115 mesh cells, with $h = 0.044mm, 0.022mm$ and $0.011mm$, respectively. The initial phase-field is given by $\varphi^0 = 1$.

Boundary conditions. We increase the displacement on Γ_{top} over time, namely we apply a time-dependent non-homogeneous Dirichlet condition:

$$u_x = t\bar{u}, \quad \bar{u} = 1 \text{ mm/s}, \tag{32}$$

where t denotes the total time. For phase-field, we prescribe homogeneous Neumann conditions on the entire boundary.

Parameters. Specifically, we use $\mu = 80.77kN/mm^2$, $\lambda = 121.15kN/mm^2$, and $G_c = 2.7N/mm$. In this example $p = 0$. The time step size is chosen as $\delta t = 10^{-4}s$. The (relative) tolerance of the augmented Lagrangian loop is $TOL_{AL} = 10^{-5}$. Furthermore, we set $\kappa = 10^{-12}h[mm]$ and $\varepsilon = 2h$.

Quantities of interest. To check the solution, we observe the crack path and in particular the time instant when the crack reaches the lower boundary. Secondly, we evaluate the surface load vector on $\Gamma_{top} := \{(x, y) \in B | 0mm \leq x \leq 10mm, y = 10mm\}$ as

$$\tau = (F_x, F_y) := \int_{\Gamma_{top}} \sigma(u)n \, ds,$$

Figure 5: Example 1: Single edge notched shear test. We prescribe the following conditions: On the left and right boundaries, $u_y = 0mm$ and traction-free in x-direction. On the bottom part, we use $u_x = u_y = 0mm$ and on Γ_{top}, we prescribe $u_y = 0mm$ and u_x as stated in (32). Finally, the lower part of the slit is fixed in y-direction, i.e., $u_y = 0mm$. We notice that the initial crack is described in the geometry by doubling the degrees of freedom on the respective faces. Consequently, the initial phase-field is $\varphi^0 = 0$ in the entire domain.

with normal vector n, and we are particularly interested in F_x. Moreover, we compare the performances of the first 6 nonlinear methods presented in Table 1.

Discussion of findings. The crack pattern at various times and the final displacement field are shown in Figure 6 and is in good agreement to other results reported in the literature, e.g., [50, 12]. The first important observation can be found in Figure 7, which shows in the left and right subfigures that independently of the specific Newton scheme, the load-displacement curve does not change. Of course this is a general hope that the numerical scheme does not change the physical result, which is indeed the case here; in Section 5.3 we however see that the numerical scheme does change the results for certain configurations. Finally, in the middle subfigure of Figure 7 we provide a comparison on three different mesh levels. These results coincide with observations made in [32, 73].
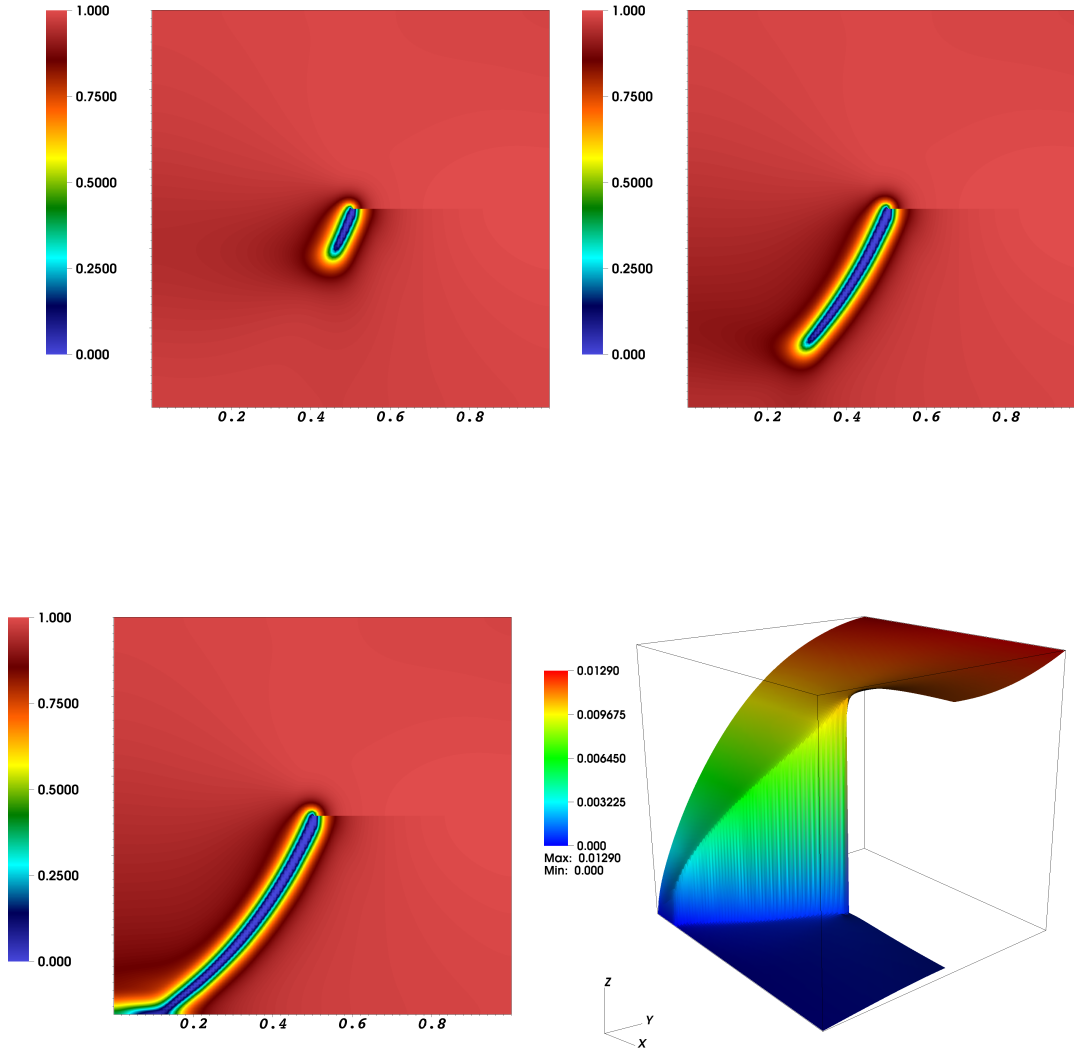
Figure 6: Example 1: Crack pattern at $T = 0.0105s, 0.0120s, 0.0130s$. The last figure shows that final displacement field at $T = 0.0130s$ and in particular the jump of displacements across the crack. Since a continuous finite element is used, the solution in the jump is continuous. However, the original given crack was built into the geometry and is therefore discontinuous.

In the following we provide a detailed study of the Newton solver performances. As it can be observed in Figure 8, except the scheme without any criterion (see Table 1), all schemes work. The most expensive schemes are clearly the Newton-like scheme $S = 0$ and the combination modified Newton with quasi-Newton steps, in which the Jacobian is not re-build at every step. This is an important observation because it limits an often-used feature (see also Remark 3.3) to reduce the computational cost of Newton methods (see e.g., [22]). In phase-field fracture it seems that the Jacobian matrix and the right hand residual should fit as well as possible and small perturbations increase significantly the computational cost. Next in the right subfigure (top) in Figure 8, we also see that the line search procedure is more efficient from time $T = 0.0108s$ than the modified Newton scheme. This holds true on coarse and finer meshes as the middle subfigure of Figure 8 displays. Finally, we perform comparisons on different meshes for both the line search and modified Newton approaches. Except when the fracture tries to reach the lower boundary, we observe very reasonable Newton iteration numbers; also in view of the iteration numbers reported in [27].

In Figure 9, we exemplarily show the behavior of several schemes in certain Newton cycles. First, we observe divergence for the method without any criterion. Next, we detect monotone, but slow convergence for $S = 0$. The line search scheme (as we already discussed) converges fastest but in a non-monotone fashion. The modified Newton scheme is highly oscillatory, but finally converges as well.
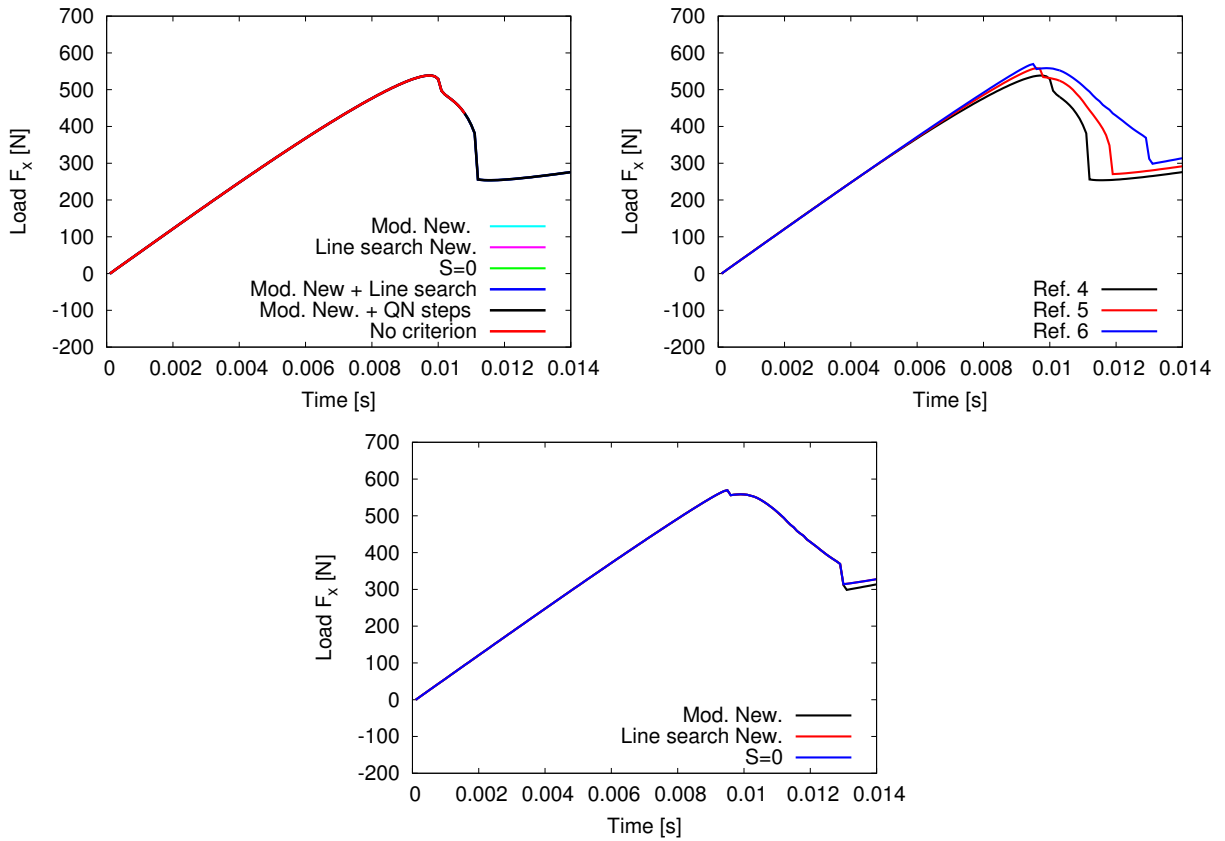
Figure 7: Example 1: Load-displacement evolution. At left, all schemes are compared on refinement level 4. In the top right subfigure, the modified Newton scheme is compared on three mesh levels. On the bottom, the three best schemes are compared on refinement level 6. In the top left figure, the important observation is that we only identify two colors: red and black. The red curve belongs to 'no criterion' and the computation fails due to a residual blow-up (see Figure 9) before the crack reaches the bottom left corner. All other computations are valid and yield the same load-displacement curve. The latter observations show that different numerical solvers do not alter the physical model and therefore, only the black curve is visible.
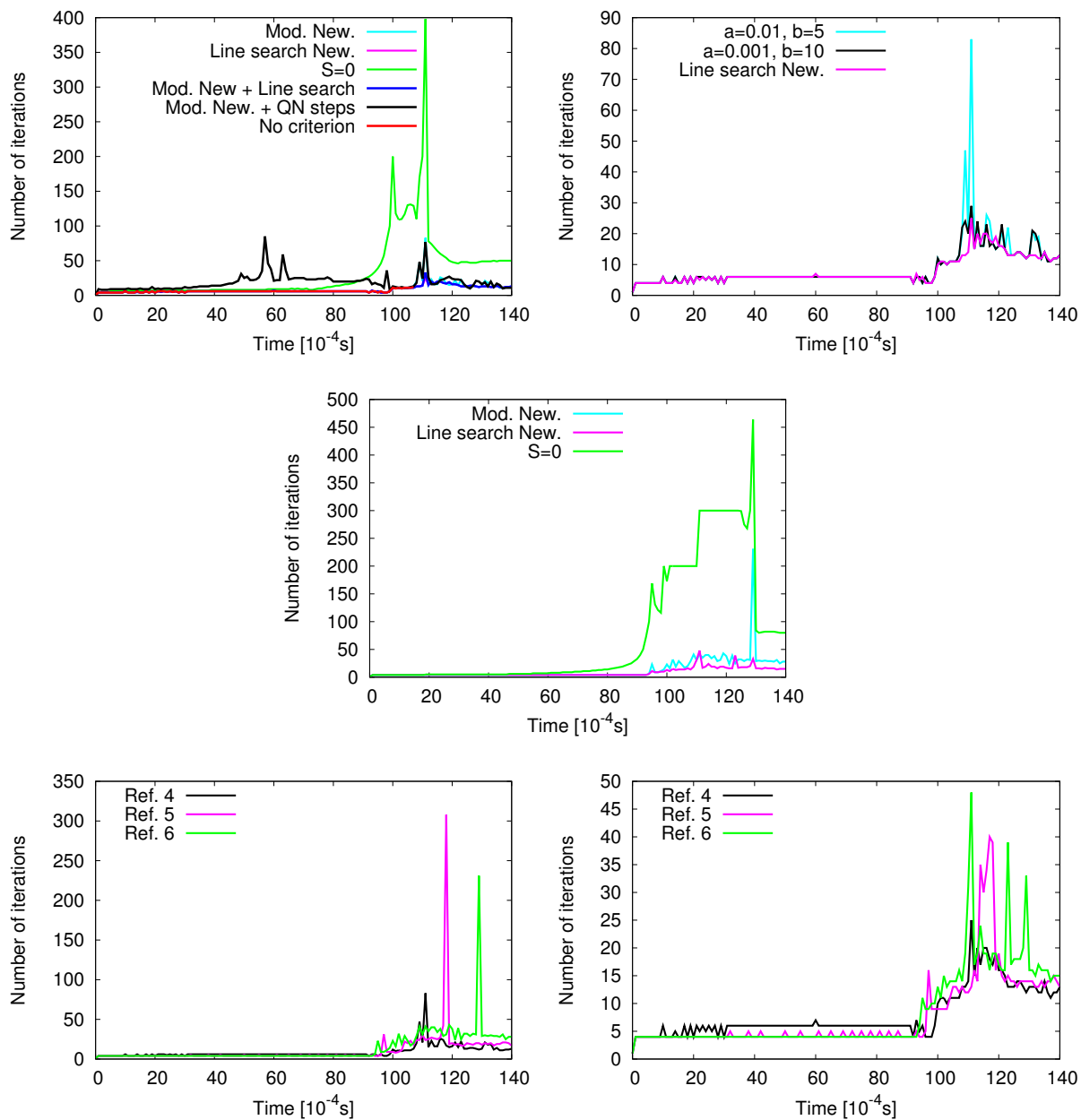
Figure 8: Example 1: Total number of Newton iterations per time step. Top: at refinement level 4 all schemes are compared and then focused on the two best schemes. Middle: Comparison of three schemes on refinement level 6. Bottom: Comparison of the modified Newton scheme for different mesh levels 4,5,6 (left) and using backtracking line search (right). In this example, the line search scheme is more efficient than the modified Newton approach.
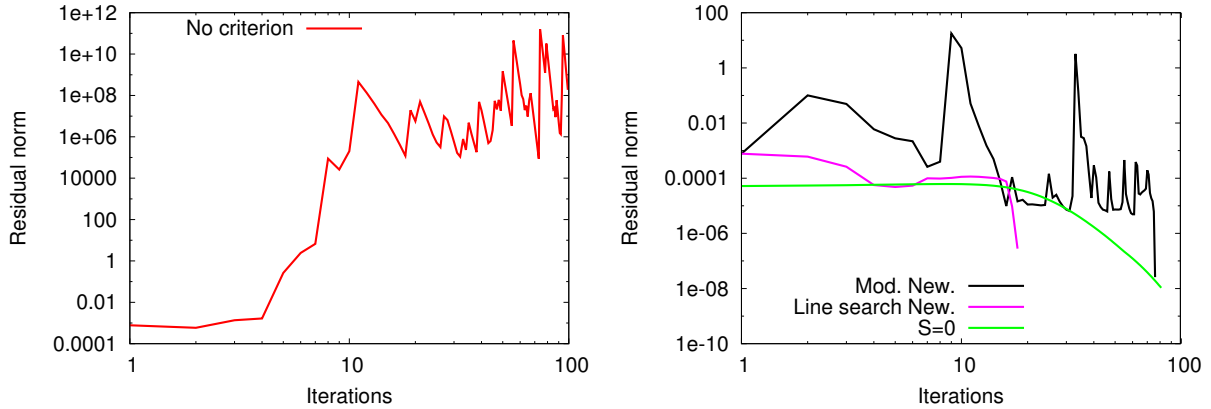
Figure 9: Example 1: Exemplary Newton divergence at $T = 0.0108s$ for the method without any criterion (left). Newton performance for the converging schemes at right at $T = 0.0111s$.

Next, we compare various choices for a and b for the modified Newton scheme in Figure 10. Here, the scheme with very small a and a moderate b works best. The schemes $a = 0.001$ and $b = 100$ that causes rapid changes in ω has the worst performance. In Figure 11, we display our findings using the line search procedure with energy monitoring. The performance is similar to a standard line search method with backtracking and both line search methods perform slightly better than the modified Newton scheme (see e.g., 11 the right subfigure) with $a = 0.001$ and $b = 10$. Moreover, observing again [27][Figures 21-23], we see a very comparable number of Newton steps and energy values (Figure 12) per loading step, from which we infer that our implementation of their scheme is correct. Finally, we study in Figure 13 the evolution of ω during the Newton iteration at the critical step 111. The worst scheme, $a = 0.001, b = 100$, shows highly oscillatory behavior. The best scheme uses moderate ω and then goes back (or close) to $\omega = 1$.
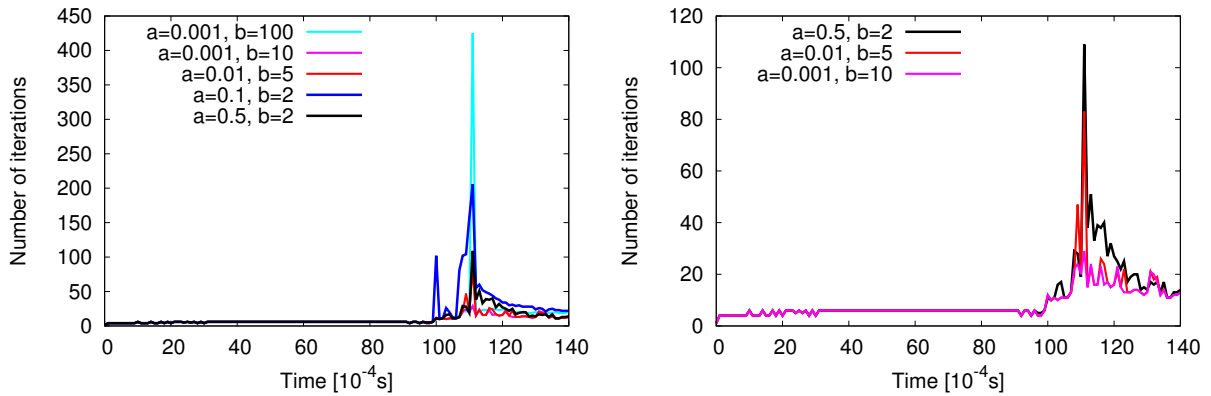
Figure 10: Example 1: Total number of Newton iterations on refinement level 4 per time step for various choices of a and b of the modified Newton scheme. At right, we focus on three configurations that perform best.

22
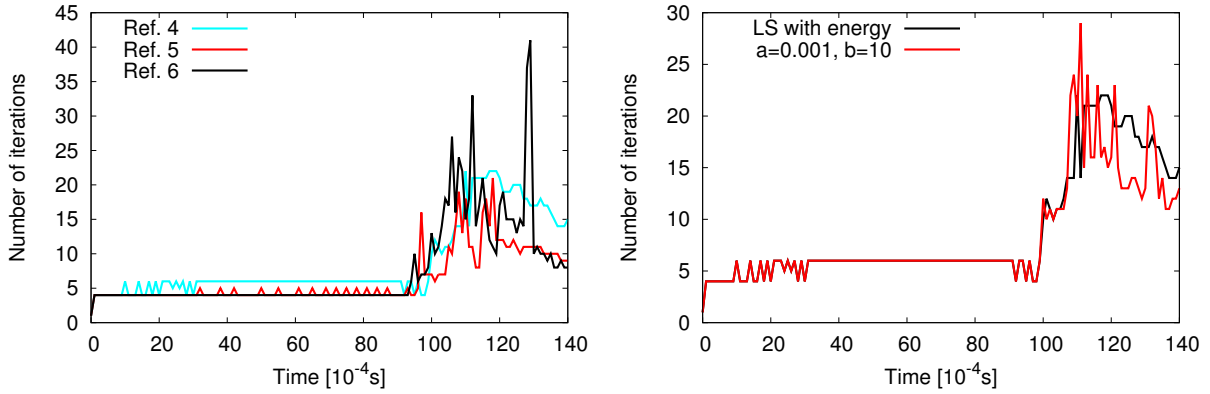
Figure 11: Example 1: Total number of Newton iterations for the line-search based method with energy monitoring (LS with energy) from Section 3.3 and comparison with the modified Newton scheme with $a = 0.001$ and $b = 10$. For this test case, both schemes show a comparable performance.
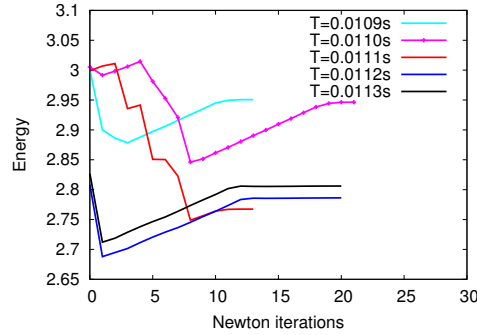
Figure 12: Example 1: Evolution of the global energy functional $E(U_k)$ during the Newton iterations k for the line-search based method with energy monitoring from Section 3.3 for the five critical steps in which the fracture reaches the bottom boundary of the specimen. The number of Newton iterations and energy values are comparable to the values published in [27]. The energy may slightly increase due to the parameter $R = 0.01$, but most importantly the final energy is lower than the initial energy at Newton step No. 0. The fracture reaches the lower boundary at $T = 0.0111s$.
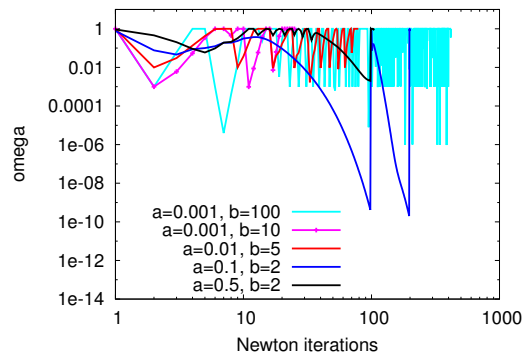
Figure 13: Example 1: Evolution of ω at time step 111 ($T = 0.0111s$) versus the total number of Newton iterations. We observe that the first choice $a = 0.001$ and $b = 100$ yields highly oscillatory behavior and is not adequate, leading to the largest number of iteration steps to converge. In general, we see that however smaller values for a, but moderate increase in b, yields a fewer number of iterations to converge. In this respect the best scheme for this test case is the choice $a = 0.0001$ and $b = 10$, which can also compete in terms of computational cost with the line search version as it can be seen in Figure 8 at top right. As final comment, we notice that all choices for a and b yield finally convergence from which we infer that the modified Newton scheme is robust with respect to these parameter choices.

23

5.2. A pressurized propagating fracture

In this second test, we consider a pressurized propagating fracture. The configuration is the same as presented in [68] and an extension of the important Sneddon/Lowengrub benchmark [63].

The characteristic feature of this test is that an initial crack is prescribed with the help of the phase-field variable. Secondly, the crack will propagate instantaneously through the entire domain.

Configuration. We deal with the following geometric data: $\Omega = (0m, 4m)^2$ and a (prescribed) initial crack with half length $l_0 = 0.2m$ on $\Omega_F = (1.8 - h, 2.2 + h) \times (2 - h, 2 + h) \subset \Omega$. The initial mesh is $6, 7$ and 8 times uniformly refined, leading to $4096, 16384$ and 65536 mesh cells, with $h = 0.088m, 0.044m$ and $0.022m$, respectively.

Boundary and initial conditions. In contrast to Example 1, the initial crack is described with the help of the phase-field function φ. We set at $t = 0$:

$$\varphi^0 = 0 \quad \text{in } \Omega_F, \quad \text{and} \quad \varphi^0 = 1 \quad \text{in } B \setminus \Omega_F. \tag{33}$$

As boundary conditions, we set the displacements to zero on $\partial\Omega$ and for the phase-field, homogeneous Neumann conditions are prescribed.

Parameters. The fracture toughness is chosen as $G_c = 1.0N/m$. The mechanical parameters are Young's modulus and Poisson's ratio $E_s = 1.0Pa$ and $\nu_s = 0.2$. The relationship to the Lamé coefficients μ_s and λ_s is given by:

$$\mu_s = \frac{E_s}{2(1 + \nu_s)}, \qquad \lambda_s = \frac{\nu_s E_s}{(1 + \nu_s)(1 - 2\nu_s)}.$$

The regularization parameters are chosen as $\varepsilon = 2h$ and $\kappa = 10^{-12}h$. Furthermore, the relative augmented Lagrangian tolerance is $TOL_{AL} = 10^{-2}$.

Input data. At each time step the pressure load p is increased as

$$p(t) = 0.1 + t \cdot 0.1, \qquad 0s \leq t \leq 14s,$$

where t denotes the current time.

Quantities of interest. We observe the length/path of the fracture as well as the number of Newton and augmented Lagrangian iterations.

Discussion of findings. The findings of this test significantly differ from published results in two ways: the final crack pattern depends on the mesh as pictured in Figure 14 and on the solver parameters (see Figure 15). However, the time point at which the crack starts propagating and reaches the boundary is the same for different solvers on the same mesh. The different crack patterns may be related to the non-uniqueness of the underlying continuous problem. It is the first time, that we observe for this configuration non-unique results, possibly thanks to the fully monolithic formulation and higher accuracy of the coupling conditions.

Comparing Figure 16 to published results in [73], it can be inferred that the modified Newton scheme is much more efficient and reliable than alternating minimization, an error-oriented Newton scheme or even the extrapolated scheme. One has to notice that the pressure for the error-oriented scheme in [73] had to be reduced in order to keep Newton's method converging. In the current study, we could use the same pressure increments as for the extrapolated scheme and the Newton iterations are still less. We finally notice that several augmented Lagrangian iterations per time step have been performed (see Figure 17). For instance at $T = 11s$, refinement level 8, we observe 338 Newton iterations, and 20 augmented Lagrangian iterations (actually this is the maximum that we allow). This means 17 Newton iterations per augmented Lagrangian iteration. In view of Section 4, these findings are not too bad. It is clear that the computational cost can be drastically reduced by weakening the tolerance for the augmented Lagrangian iteration. Such a study (for the screw tension test), including possible pitfalls, has been provided in [73]. In Figure 18, we observe ω for different choices of a and b. For smaller a, the control parameter ω becomes very small at the critical times $T = 11s$ and $T = 12s$.

Finally, we ran several tests using the line-search procedure described in Section 3.3. In comparison to Example 1, we could not achieve satisfactory results. Depending on the number of Newton steps and augmented Lagrangian steps, the final number of iterations was not at all competitive. On the other hand, we also tested various modifications of the energy functional (14) in Step 3 in Algorithm 3.2. For instance, the full version would accept Newton updates in which at $T = 12s$ the fracture completely vanishes, i.e., $\varphi = 1$, with the result that $E(U) \approx 0$, which is, of course, admissible from the energy point of view (recall our findings in Section 4 in Figure 3). We then tested a simplified version by observing only the bulk energy in the convergence monitor. Here, we obtain the same crack pattern as displayed in Figure 14, but with more Newton steps. In all tests, we also observed that negative line search parameters were taken, but which only partially yielded results. We also had test cases in which no final convergence could be reached. These observations coincide with the statement in [61] that the correct choice of negative search directions may become challenging. We have not yet found a final solution to this problem. In consequence, in view of all results obtained in this subsection and [73][Section 5.4], we conclude that using a fully monolithic scheme, only the modified Newton method seems to yield reliable results for this setting.
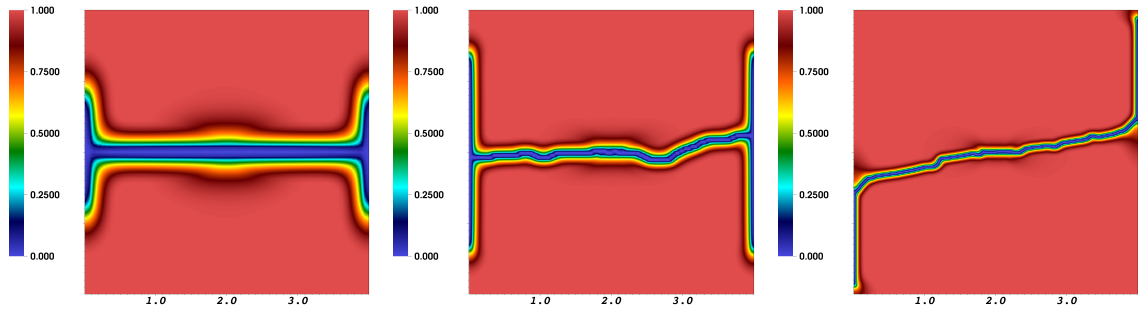
Figure 14: Example 2: Crack pattern for the modified Newton scheme ($a = 0.01, b = 5$) on three refinement levels at times $T = 11$ (refinement level 6), $T = 12$ (refinement level 7), $T = 13$ (refinement level 8). The final crack path is mesh-dependent (but also possibly on solver settings) and the propagation slightly is shifted towards later times when refining the mesh.
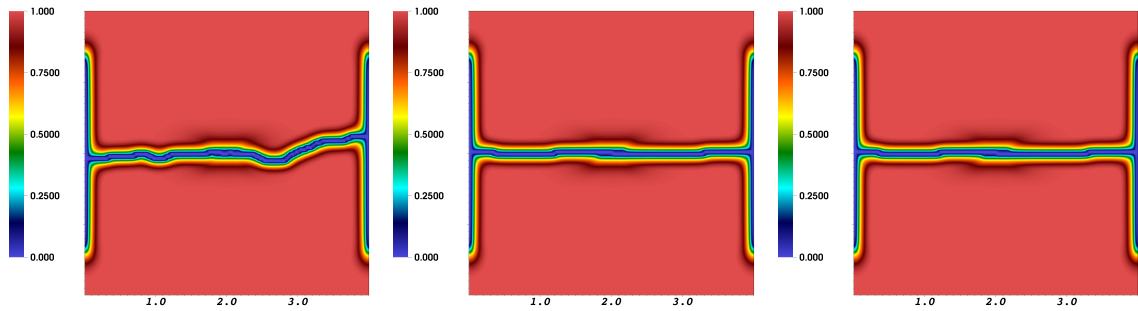
Figure 15: Example 2: Crack pattern on refinement level 7 and $T = 12$ but different solvers: modified Newton with $a = 0.01, b = 5$ (left), $a = 0.1, b = 2$ (middle) and $S = 0$ (right).

25
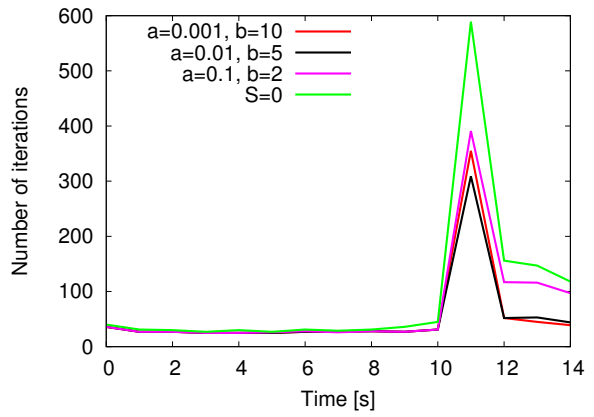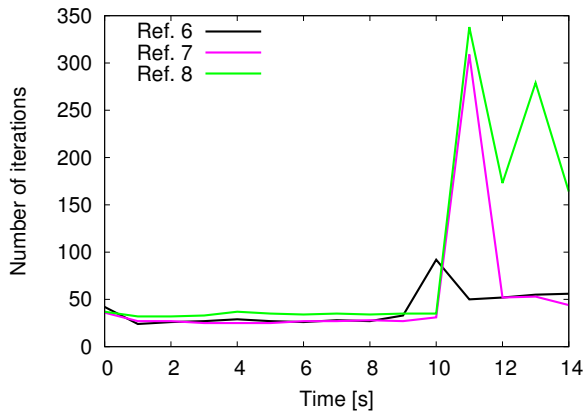
Figure 16: Example 2: Comparison of the total number of Newton iterations for the modified scheme with $a = 0.01$ and $b = 5$ (left). On refinement level 7 we compare four different schemes (right subfigure). These total numbers must be put into relation with the augmented Lagrangian iterations per time step. Specifically, to get a more realistic idea, per time step the number of Newton steps must be divided by the corresponding number of augmented Lagrangian iterations provided in Figure 17.
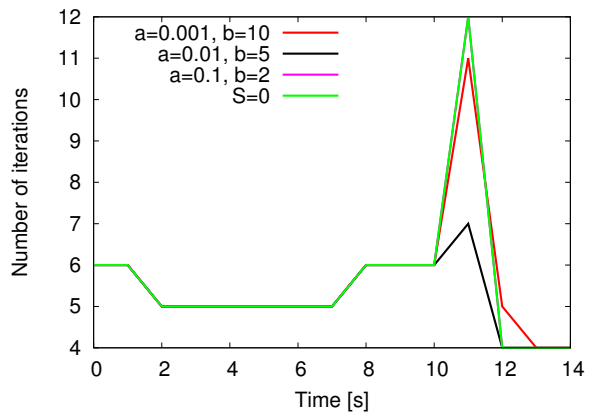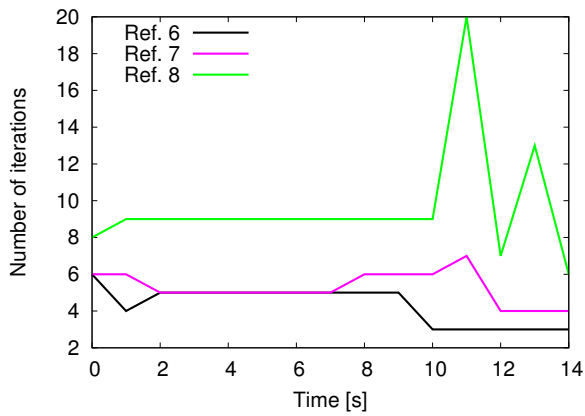
Figure 17: Example 2: Comparison of the total number of augmented Lagrangian iterations for the modified scheme with $a = 0.01$ and $b = 5$ (left). On refinement level 7 we compare four different schemes (at right).
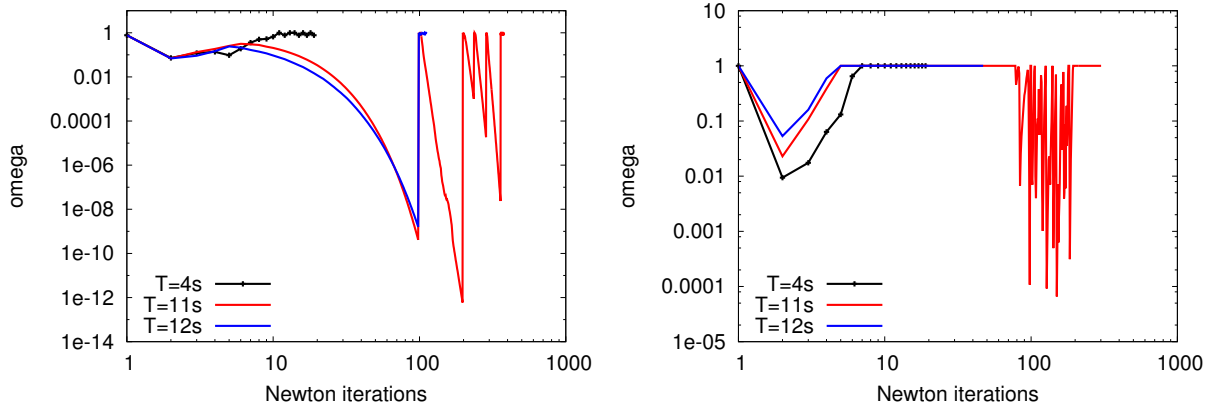
Figure 18: Example 2: Evolution of ω at three different times $T = 4, 11, 12s$ for two parameter choices $a = 0.1$ and $b = 2$ (left) and $a = 0.01$ and $b = 5$ (right). We observe that the first choice at left, leads in certain steps to very small $\omega \approx 0$, whereas for the latter choice, the smallest ω is of the order 10^{-4}. Apart from these critical steps at $T = 11s$ and $T = 12s$, the modified Newton scheme requires in general smaller ω at the beginning of the Newton iteration and then goes back to full Newton steps as exemplarily shown for $T = 4s$. These observations hold true for all $0s \le T \le 10s$, but are not shown here, except for $T = 4s$.

5.3. Screw tension tests

This third test is split into two subtests. In contrast to the previous examples, no initial fracture is prescribed in the first subtest. Rather, a fracture will develop due to high stresses, which highlights that the phase-field model indeed recognizes high stress regions in which the material will damage. For theoretical work on crack nucleation in brittle materials we refer the reader to [20, 65].

In the second test, an initial fracture is prescribed representing a hollow-rolled screw motivated by experimental data [69]. Therein two hollow-rolled scenarios are considered: a short crack with $3mm$ initial length and a long crack with $6mm$ initial length.

Configuration. The geometric setting is displayed in Figure 19. The total length is $17.20mm$. The initial mesh is once uniformly refined yielding 13760 mesh elements.

Initial conditions. In Example 3a, the initial screw is undamaged and therefore $\varphi^0 = 1$ in B. In Example 3b (short), an initial crack with the help of the phase-field variable is prescribed along $\Omega_F = \{x = 0 \pm 2h; -10mm \le y \le -7mm\}$, thus $\varphi^0 = 0$ in Ω_F. In Example 3b (long), an initial crack with the help of the phase-field variable is prescribed along $\Omega_F = \{x = 0 \pm 2h; -13mm \le y \le -7mm\}$, thus $\varphi^0 = 0$ in Ω_F.

Boundary conditions. Crack growth is driven by a non-homogeneous Dirichlet condition for the displacement field u on Γ_{top}, the head of the screw at $y = 0.0$. We increase the displacement on Γ_{top} at each time step such that the head is pulled, namely

$$u_y = \delta t \times \bar{u}, \quad \bar{u} = 1.0 \text{ mm},$$

where $\delta t = 10^{-2}$s.
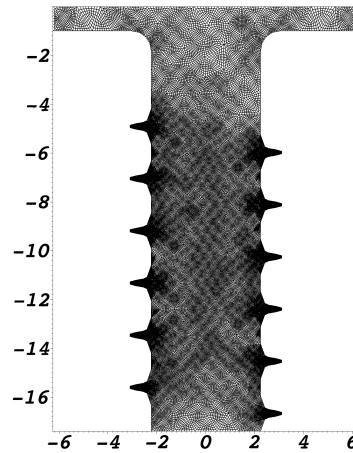
Figure 19: Example 3: Mesh of screw simulations. The screw is fixed at the bottom, at top we have non-homogeneous Dirichlet conditions in y-direction (uniform tension). The units are in *mm*.

Parameters. As model parameters, we choose $\gamma = 1$, $\kappa = 10^{-10}h$, $\epsilon = 2h$ mm. We notice that the maximum number of possible augmented Lagrangian iterations is 20 and $TOL_{AL} = 10^{-3}$. The total time is not specified a priori but rather by the fact when the screw is damaged. The time step size is $\delta t = 0.01s$. As material parameters, we use $\mu = 80.77kN/mm^2$, $\lambda = 121.15kN/mm^2$ and $G_c = 2.7N/mm$. As in Example 1, we set $p = 0$.
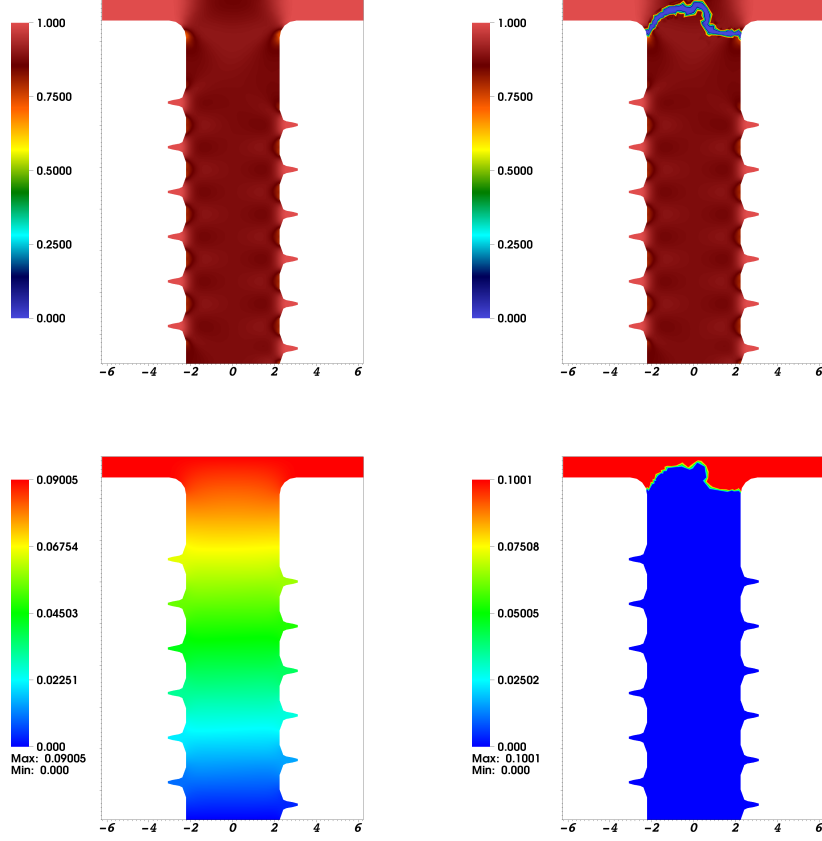
Figure 20: Example 3a: Crack pattern (top) and vertical displacements (bottom) at $T = 0.1s$ and $T = 0.11s$ using the modified Newton scheme with $a = 0.01, b = 5$.

Quantities of interest. We observe the crack patterns and vertical displacement fields. Furthermore, we study the evolution of the bulk and crack energies (extracted from (14)):

$$E_B = \int_\Omega ([1 - \kappa]\varphi^2 + \kappa)\psi(e) \, dx, \tag{34}$$

and

$$E_C = \frac{G_c}{2} \int_\Omega \left(\frac{(\varphi - 1)^2}{\varepsilon} + \varepsilon|\nabla\varphi|^2 \right) dx, \tag{35}$$

with the strain energy functional

$$\psi(e) := \mu\mathrm{tr}(e(u)^2) + \frac{1}{2}\lambda\mathrm{tr}(e(u))^2, \quad \text{with } e := e(u) := \frac{1}{2}(\nabla u + \nabla u^T),$$

and $|\nabla\varphi|^2 := \nabla\varphi \cdot \nabla\varphi$. Finally, we study Newton iteration numbers and Newton's behavior at selected time steps.

28

Discussion of findings. We infer from the Figures 20, 21, 22, and 23 that these results differ in comparison to alternating minimization [69] and the quasi-monolithic method [73]. As in the previous example, we observe an immediate and instantaneous crack explosion (propagation). For better quantification of these results, we plot in Figure 24 the respective energies. Therein, we observe very well that indeed the material is completely broken since the bulk energy drops to zero.
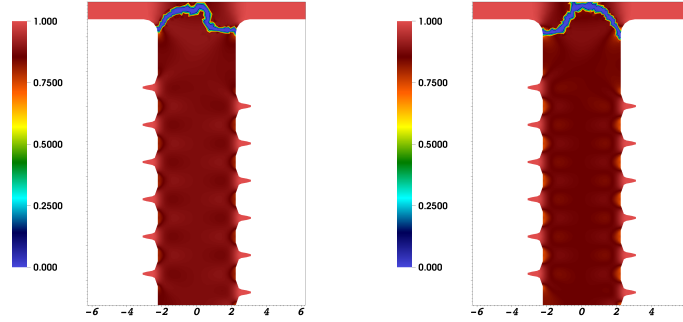
Figure 21: Example 3a: Crack pattern at $T = 0.11s$ using the modified Newton scheme with $a = 0.01, b = 5$ (left) and at $T = 0.12s$ for $S = 0$ (right). Depending on the solver, the final crack patterns differ and are not unique. However, they appear at the same time instance. Moreover, these patterns differ significantly in time and path from the results obtained in [73].
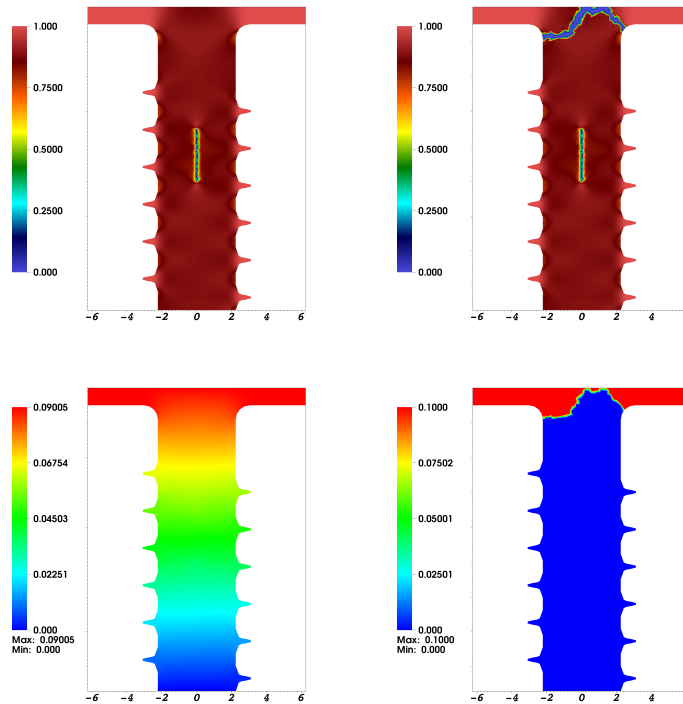
Figure 22: Example 3b (short hollow-rolled): Crack pattern (top) and vertical displacements (bottom) at $T = 0.1s$ and $T = 0.11s$ using the modified Newton scheme with $a = 0.01, b = 5$. These results again differ significantly in time and crack path from the results in [73] using an extrapolated scheme and [69] in which alternating minimization was adopted. Most importantly, the screw will not anymore break in the middle due to the hollow-rolled region but again on the head as in Example 3a.

29

Most significantly, the final crack patterns differ significantly from previous findings. The differences are with respect to the time point when the material breaks (earlier than in alternating minimization or extrapolation because the coupling conditions are tighter due to monolithic coupling). In addition, this test shows the non-uniqueness in terms of different final crack paths since fractures will develop instantaneously and depend on tolerances and stopping criteria.

In Example 3a, similar to the simplified study in Section 4, the best performance is obtained by setting the parameter $S = 0$ (see left subfigure of Figure 25), thus removing constantly the entire second block in the first line of the Jacobian. However, in Example 3b, $S = 0$ does also fail. The line search Newton scheme does not work from the very first time step on as it is highlighted in the middle figure of Figure 25. In order to further substantiate our observations from Example 1 (Section 5.1), we provide another test in which the combination of the modified Newton scheme with line-search is not very efficient as confirmed by the left subfigure of Figure 25. Finally, we observe a dramatic behavior of Newton's method in Figure 26. The initial residual is 10^2 and then goes up to 10^7 and then drops until the tolerance 10^{-7}. Thus, there is a variation of 10^{14} in the residual norm for successfully computing one time step.
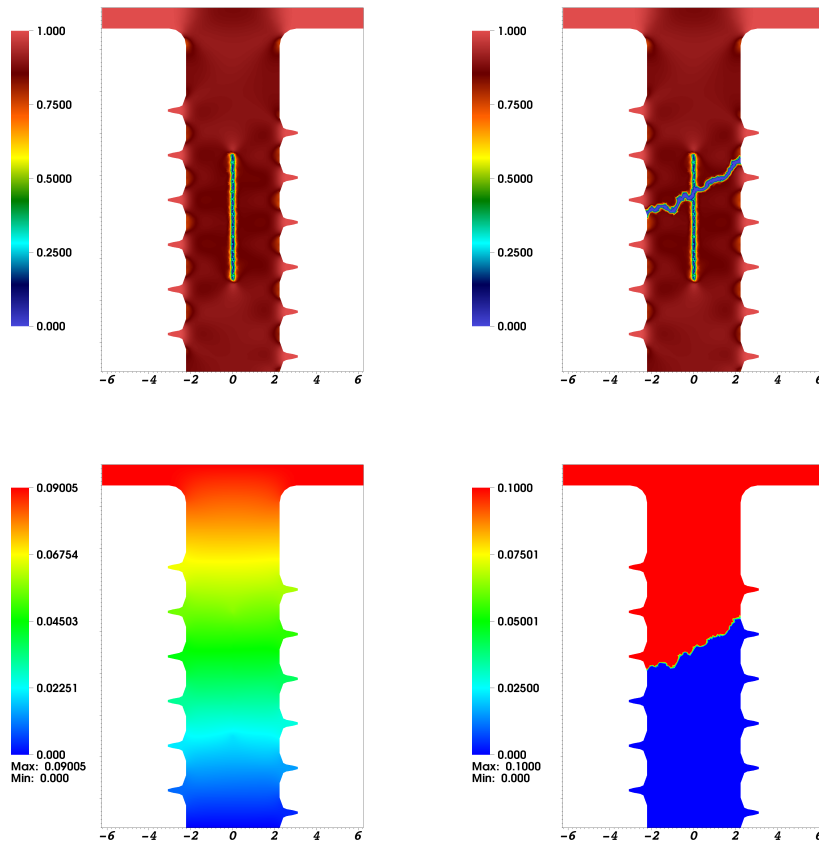
Figure 23: Example 3b (long hollow-rolled): Crack pattern (top) and vertical displacements (bottom) at $T = 0.1s$ and $T = 0.11s$ using the modified Newton scheme with $a = 0.01, b = 5$. Here, we observe similar to [69] that the screw will be cracked in the middle. Obviously, the length of the damaged zone has an impact where the screw will totally damage under tension.
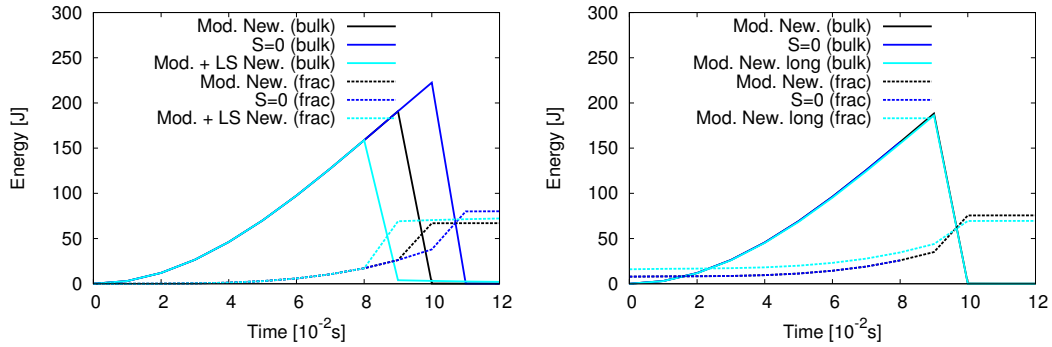
Figure 24: Example 3a/b: evolution of the bulk and crack energies. The drop of the bulk energy characterizes crack growth. Once the bulk energy is zero, the screw is totally cracked. Therefore, from the instant of time of total damage the respective energies should remain constant, which is nicely shown by the computation of further time steps until $T = 0.12s$. In addition, in Example 3a, we observe a dependence of crack growth on the numerical solver because the bulk energy decrease happens at different time points.
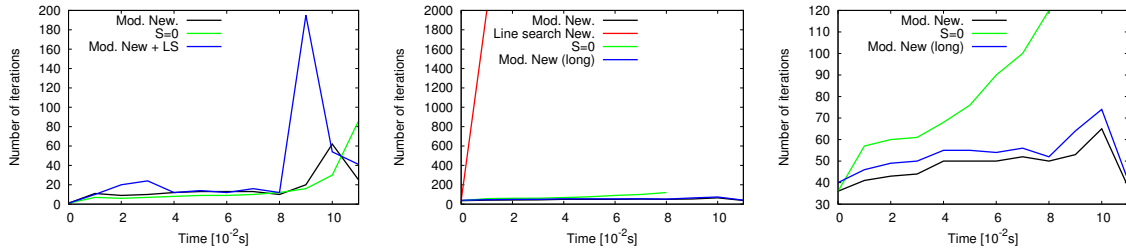
Figure 25: Example 3: Comparison of the total number of Newton iterations. At left the screw without any initial crack. In the middle and on the right, the Newton performance of the hollow-rolled screw is shown.
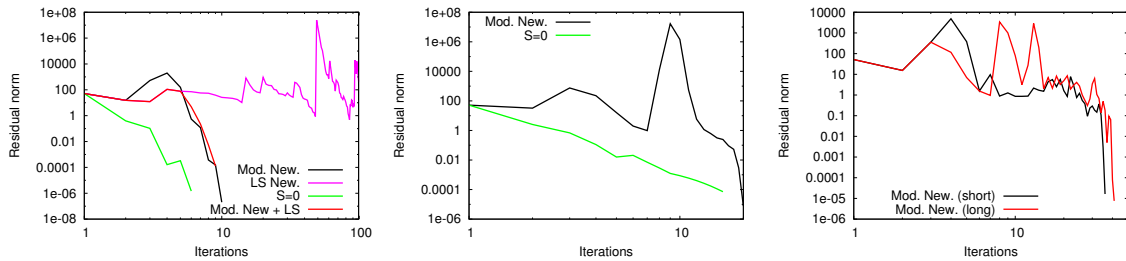
Figure 26: Example 3: Exemplary performance of Newton's method for the screw without crack at $T = 1s$ and $T = 9s$ (left and middle, respectively). At right, the performances at $T = 10s$ for both hollow-rolled screws are shown.

31

5.4. Two 3D situations with two interacting fractures

In this final example we investigate again two subtests, but now in three dimensions. In the first subtest, Young's modulus is constant. In the second subtest, Young's modulus is cell-wise different yielding a heterogeneous material. Since the computational cost is immediately high, we implemented local mesh refinement. We consider two initial fractures which are subject to increasing pressure. In this test, we study various parameter choices for the modified Newton method.

Configuration. We work in the cube $B = (0, 10)^3$. Two initial fractures are located at $\Omega_{F1} = \{x = 2.6 \pm h; 3.8 \leq y \leq 5.5; z = 4 \pm h\}$ and $\Omega_{F2} = \{5.5 \leq x \leq 7; y = 4 \pm h; z = 6 \pm h\}$. The initial geometry is two times uniformly refined and three times locally in the subcube $B_{sub} = (3, 7)^3$. This yields 8576 mesh elements and 40364 degrees of freedom. The smallest h is $h_{min} = 0.54m$.
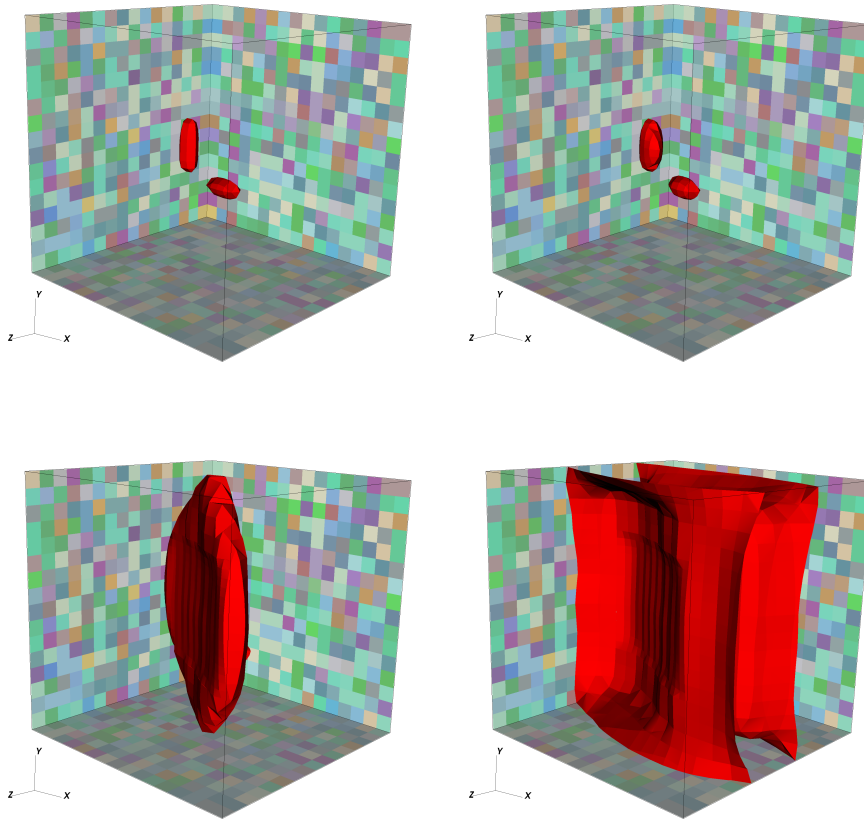
Figure 27: Example 4: Crack pattern at different times $T = 0, 8, 9, 12s$. The crack suddenly grows as in the two previous examples.

Parameters. The time step size is $\delta t = 1s$ and we compute until the end time $T = 14s$. Young's modulus is $E = 5Pa$ for the homogeneous material test case and $E \in [2, 10]Pa$ for the heterogeneous material test case. Poisson's ratio is $\nu_s = 0.2$. Furthermore $G_c = 1.0N/m$. Moreover, $\gamma = 100$ and $\kappa = 10^{-10}h, \epsilon = 2h_{min}$. The relative augmented Lagrangian tolerance is $TOL_{AL} = 10^{-3}$, but at maximum 3 iterations in order to keep the computational cost reasonable (we perform however two tests with maximal 10 iterations for comparisons).

Input data. The pressure is linearly increasing:

$$p(t) = 0.001 + t \cdot 0.25.$$

Quantities of interest. In this example, we observe the fracture pattern, and study various choices of *a* and *b* and their influence on the performance of the nonlinear solver.

Discussion of findings. The crack evolution is displayed in Figure 27. As in the two previous examples, the crack will not significantly develop, but explode from $T = 8s$ to $T = 9s$. Clearly, the Newton iterations numbers then go up as observed in Figure 28. In $T = 9s$, the fracture reaches the boundary and the physical meaning of the further crack patterns are clearly questionable because of the boundary influence. Nevertheless we compute further until $T = 12s$ to observe whether the computation continues and to study further the Newton performance. Then in Figure 29, we allow for more augmented Lagrangian iterations and also study Newton's behavior at the critical time (at which the crack explodes).
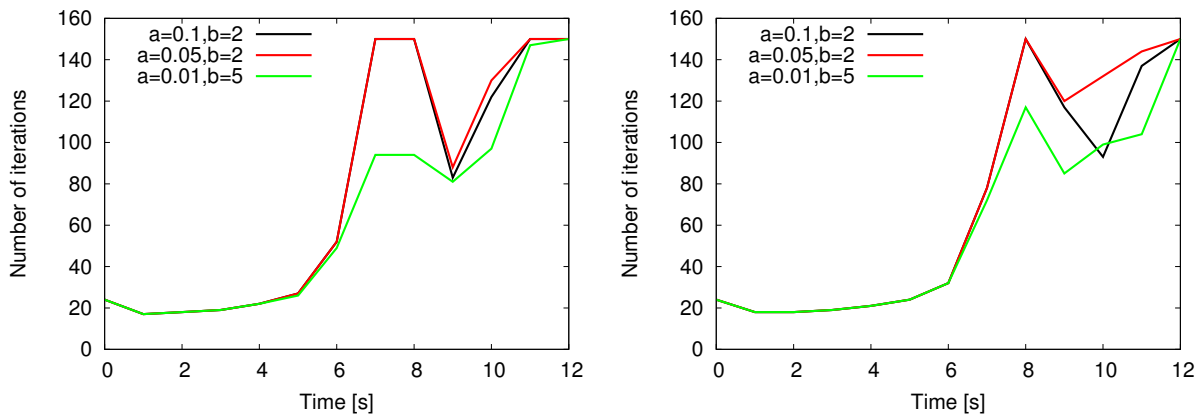
Figure 28: Example 4: Total number of Newton iterations per time step. At each time step, also three augmented Lagrangian iterations are performed such that in average at each time step 1/3 of the above numbers are required for solving the system per augmented Lagrangian step.
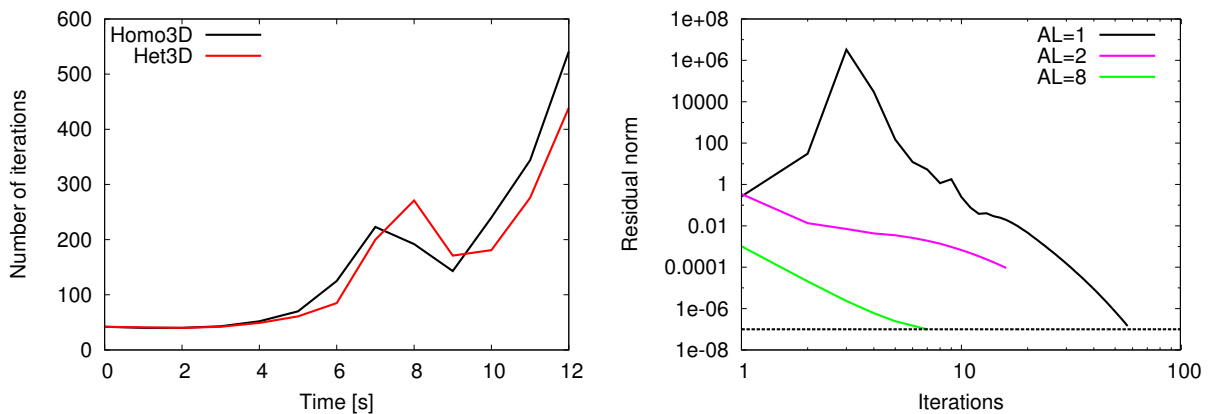
Figure 29: Example 4: Total number of Newton iterations per time step in which 10 maximum augmented Lagrangian iterations are allowed per time step (left). At right, for the homogeneous test case, the performance of Newton's method at the critical time $T = 8s$ is shown. Here, convergence patterns for three different augmented Lagrangian iterations are shown. Clearly, with each augmented Lagrangian iteration, the solution is improved and Newton's method needs less steps to converge. For the first two AL iterations, the final tolerance is not reached because of the adaptive choice of Newton's tolerance (see Section 4 in [73]).

33

6. Conclusions

In this paper, we further developed Newton algorithms for solving nonlinearly coupled variational phase-field fracture problems in a monolithic fashion. A novel algorithm is based on a dynamic modification of the Jacobian matrix depending on the fraction of the current residual in comparison to the previous residual. This idea was inspired from nonlinear fluid flow problems. For better understanding of the idea and the algorithm and its possible behavior, a simplified, but characteristic problem was studied in Section 4. This problem already shows high Newton iterations numbers despite its simplicity. In the final section, several numerical tests have been performed. Here, line-search Newton algorithms are compared to modified Newton schemes. All these configurations have particular characteristics, which we recapitulate in the following.

6.1. Summaries of the numerical examples

In Example 1, the single edged notched shear test, an initial crack was built into the geometry and then a phase-field fracture will slowly develop. Here, we observed that line-search-based Newton performed as reliable as the modified Newton scheme with dynamic Jacobian modification. Moreover, the line-search scheme with energy monitoring proposed in [27] yielded similar performance. We also found that the common strategy to reduce the computational cost by introducing quasi-Newton steps is not advisable for phase-field fracture due to the strong coupling the displacements and phase-field variable. In these cases, the numerical perturbation between the Jacobian matrix and the right hand side residual becomes too large causing Newton's method to diverge. In the second example, a pressurized propagating fracture, an initial crack with the help of the phase-field function was prescribed. Here at some point, the fracture will propagate extremely fast and the final crack patterns depend on the mesh and on the solver parameters. In this example, the modified Newton scheme with dynamic Jacobian modification yields very good findings, whereas an error-oriented version works as well, but is not efficient at all [73]. In Example 3, a screw test, fracture nucleation in the region of the highest stresses is the key characteristic feature of this test. Here, the error-oriented Newton method will not work [73] and also a backtracking line search Newton method fails. The modified Newton scheme yields excellent results and therefore we could close the gap that fully monolithic schemes would previously not work for this test case. Moreover, similar to Example 2, the final crack pattern differ depending on the chosen Newton parameters. In the final example, we addressed a 3D configuration in homogeneous and heterogeneous media. Also here, we observed extremely fast crack growth and reasonable Newton iteration numbers.

6.2. Final analysis, interpretation and outlook

In summary, we draw the conclusion that, first, the fully monolithic solution of phase-field fracture, due to the nonlinearities and non-convexity remains extremely challenging. Secondly, the performance of the algorithms is problem-dependent. Indeed, the modified Newton scheme is not the most efficient scheme in some tests, but most importantly the method is robust. In all tests the chosen parameters $a = 0.01$ and $b = 5$ would yield results independently of the configuration, material parameters, input data, time steps, and mesh sizes. Thus it was not necessary to 'tune' for each configuration these solver parameters. On the other hand, we have chosen a range of different parameters a and b in the Examples 1 and 2 in which the influence on the Newton solver becomes significant, but still all choices for a and b would work.

Specifically, the last three examples with very fast crack growth exhibited a high number of Newton iterations at the moment where the crack starts growing (i.e., exploding). But these numbers seem reasonable in view of the complexity of the underlying problem. Importantly, the computational cost is (significantly) lower than seen in other results [73]. Moreover, these results also differ observing the quantities of interest. Crack growth happens earlier and faster and consequently, the crack velocity is different in particular in comparison to alternating minimization and an extrapolated scheme.

The achievement of having a robust Newton solver available, allows us now to further increase the efficiency of numerical simulations of phase-field fracture problems and its informative value. Possible immediate applications are further improvements and studies on parallel computations, multiphysics fracture, adjoint-based a posteriori error estimation and gradient-based optimization. We finally notice that the very fast crack growth in the last three examples raises the question whether a quasi-static model is still sufficient or a dynamic fracture model would be more appropriate. We will work on this question in future studies as well.

Acknowledgments

I want to thank Thomas Richter (Univ. Magdeburg) who pointed me to Mandal's et al. paper [45]. Furthermore, I thank Luca Lena Jansen and Jonas van Stappen (both École Polytechnique) for inspiring discussions and for providing their octave/MATLAB code developed in [37], which I then could further extend for the computations carried out in Section 4. Next, I thank the authors of [27] (Tymofiy Gerasimov and Laura De Lorenzis) for answering my questions with regard to their proposed line-search version. Finally, I want to thank the anonymous reviewers for their careful reading and interesting questions.

References

[1] G. Allaire, F. Jouve, and N. V. Goethem. Damage and fracture evolution in brittle materials by shape optimization methods. *Journal of Computational Physics*, 230(12):5010 – 5044, 2011.

[2] M. Ambati, T. Gerasimov, and L. de Lorenzis. Phase-field modeling of ductile fracture. *Comput. Mech.*, 2015.

[3] M. Ambati, T. Gerasimov, and L. De Lorenzis. A review on phase-field models of brittle fracture and a new fast hybrid formulation. *Computational Mechanics*, 55(2):383–405, 2015.

[4] M. Ambati and L. D. Lorenzis. Phase-field modeling of brittle and ductile fracture in shells with isogeometric nurbs-based solid-shell elements. *Computer Methods in Applied Mechanics and Engineering*, 312:351 – 373, 2016. Phase Field Approaches to Fracture.

[5] L. Ambrosio and V. Tortorelli. Approximation of functionals depending on jumps by elliptic functionals via γ-convergence. *Comm. Pure Appl. Math.*, 43:999–1036, 1990.

[6] L. Ambrosio and V. Tortorelli. On the approximation of free discontinuity problems. *Boll. Un. Mat. Ital. B*, 6:105–123, 1992.

[7] H. Amor, J.-J. Marigo, and C. Maurini. Regularized formulation of the variational brittle fracture with unilateral contact: Numerical experiments. *J. Mech. Phys. Solids*, 57:1209–1229, 2009.

[8] M. Artina, M. Fornasier, S. Micheletti, and S. Perotto. Anisotropic mesh adaptation for crack detection in brittle materials. *SIAM J. Sci. Comput.*, 37(4):B633–B659, 2015.

[9] W. Bangerth, R. Hartmann, and G. Kanschat. deal.II – a general purpose object oriented finite element library. *ACM Trans. Math. Softw.*, 33(4):24/1–24/27, 2007.

[10] W. Bangerth, T. Heister, and G. Kanschat. *Differential Equations Analysis Library*, 2012.

[11] M. J. Borden, T. J. Hughes, C. M. Landis, and C. V. Verhoosel. A higher-order phase-field model for brittle fracture: Formulation and analysis within the isogeometric analysis framework. *Computer Methods in Applied Mechanics and Engineering*, 273(0):100 – 118, 2014.

[12] M. J. Borden, C. V. Verhoosel, M. A. Scott, T. J. R. Hughes, and C. M. Landis. A phase-field description of dynamic brittle fracture. *Comput. Meth. Appl. Mech. Engrg.*, 217:77–95, 2012.

[13] B. Bourdin. Numerical implementation of the variational formulation for quasi-static brittle fracture. *Interfaces and free boundaries*, 9:411–430, 2007.

[14] B. Bourdin, G. Francfort, and J.-J. Marigo. Numerical experiments in revisited brittle fracture. *J. Mech. Phys. Solids*, 48(4):797–826, 2000.

[15] B. Bourdin, G. Francfort, and J.-J. Marigo. The variational approach to fracture. *J. Elasticity*, 91(1–3):1–148, 2008.

[16] B. Bourdin, C. Larsen, and C. Richardson. A time-discrete model for dynamic fracture based on crack regularization. *Int. J. Frac.*, 168(2):133–143, 2011.

[17] B. Bourdin, J.-J. Marigo, C. Maurini, and P. Sicsic. Morphogenesis and propagation of complex cracks induced by thermal shocks. *Phys. Rev. Lett.*, 112:014301, Jan 2014.

[18] S. Burke, C. Ortner, and E. Süli. An adaptive finite element approximation of a variational model of brittle fracture. *SIAM J. Numer. Anal.*, 48(3):980–1012, 2010.

[19] S. Burke, C. Ortner, and E. Süli. An adaptive finite element approximation of a generalized Ambrosio-Tortorelli functional. *M3AS*, 23(9):1663–1697, 2013.

[20] A. Chambolle, A. Giacomini, and M. Ponsiglione. Crack initiation in brittle materials. *Arch. Ration. Mech. Anal.*, 188:309–349, 2008.

[21] P. G. Ciarlet. *The finite element method for elliptic problems*. North-Holland, Amsterdam [u.a.], 2. pr. edition, 1987.

[22] P. Deuflhard. *Newton Methods for Nonlinear Problems*, volume 35 of *Springer Series in Computational Mathematics*. Springer Berlin Heidelberg, 2011.

[23] C. Engwer and L. Schumacher. A phase field approach to pressurized fractures using discontinuous galerkin methods. *Mathematics and Computers in Simulation*, pages –, 2016.

[24] P. E. Farrell and C. Maurini. Linear and nonlinear solvers for variational phase-field models of brittle fracture. *Int. J. Numer. Meth. Engrg.*, 109:648–667, 2017.

[25] M. Fortin and R. Glowinski. *Augmented Lagrangian Methods: Applications to the Numerical Solution of Boundary Value Problems*. Stud. Math. Appl. 15. North Holland, Amsterdam, 1983.

[26] G. Francfort and J.-J. Marigo. Revisiting brittle fracture as an energy minimization problem. *J. Mech. Phys. Solids*, 46(8):1319–1342, 1998.

[27] T. Gerasimov and L. D. Lorenzis. A line search assisted monolithic approach for phase-field computing of brittle fracture. *Computer Methods in Applied Mechanics and Engineering*, 312:276 – 303, 2016. Phase Field Approaches to Fracture.

[28] R. Glowinski and P. L. Tallec. *Augmented Lagrangian and Operator-Splitting Methods in Nonlinear Mechanics*. SIAM Stud. Appl. Math. 9. SIAM, Philadelphia, 1989.

[29] D. Goldfarb. Curvilinear path steplength algorithms for minimization which use directions of negative curvature. *Mathematical Programming*, 18:31–40, 1980.

[30] A. A. Griffith. The phenomena of rupture and flow in solids. *Philos. Trans. R. Soc. Lond.*, 221:163–198, 1921.

[31] Y. Heider and B. Markert. A phase-field modeling approach of hydraulic fracture in saturated porous media. *Mechanics Research Communications*, pages –, 2016.

[32] T. Heister, M. F. Wheeler, and T. Wick. A primal-dual active set method and predictor-corrector mesh adaptivity for computing fracture propagation using a phase-field approach. *Comp. Meth. Appl. Mech. Engrg.*, 290(0):466 – 495, 2015.

[33] C. Hesch, A. Gil, R. Ortigosa, M. Dittmann, C. Bilgen, P. Betsch, M. Franke, A. Janz, and K. Weinberg. A framework for polyconvex large strain phase-field methods to fracture. *Computer Methods in Applied Mechanics and Engineering*, 317:649 – 683, 2017.

[34] C. Hesch, S. Schu, M. Dittmann, M. Franke, and K. Weinberg. Isogeometric analysis and hierarchical refinement for higher-order phase-field models. *Computer Methods in Applied Mechanics and Engineering*, 303:185 – 207, 2016.

[35] M. Hofacker and C. Miehe. Continuum phase field modeling of dynamic fracture: variational principles and staggered FE implementation. *Int. J. Fract.*, 178:113–129, 2012.

[36] J. Hron, A. Ouazzi, and S. Turek. A computational comparison of two FEM solvers for nonlinear incompressible flow. In *Lecture notes in Computational Science and Engineering, Vol. 35*, pages 87–109. Springer, 2003.

[37] L. Jansen and J. van Stappen. Newton's method for non-linear coupled systems inspired by load flow analysis. Project in numerical modeling, MAP 502, Ecole Polytechnique, March 2017.

[38] S. H. John W. Eaton, David Bateman and R. Wehbring. *GNU Octave version 3.8.1 manual: a high-level interactive language for numerical computations*. CreateSpace Independent Publishing Platform, 2014. ISBN 1441413006.

[39] C. Kuhn and R. Müller. A new finite element technique for a phase field model of brittle fracture. *Journal of Theoretical and Applied Mechanics*, 49(4):1115–1133, 2011.

[40] C. J. Larsen. *IUTAM Symposium on Variational Concepts with Applications to the Mechanics of Materials: Proceedings of the IUTAM Symposium on Variational Concepts with Applications to the Mechanics of Materials, Bochum, Germany, September 22-26, 2008*, chapter Models for Dynamic Fracture Based on Griffith's Criterion, pages 131–140. Springer Netherlands, Dordrecht, 2010.

[41] C. J. Larsen, C. Ortner, and E. Süli. Existence of solutions to a regularized model of dynamics fracture. *Methods in Applied Sciences*, 20:1021–1048, 2010.

[42] S. Lee, J. E. Reber, N. W. Hayman, and M. F. Wheeler. Investigation of wing crack formation with a combined phase-field and experimental approach. *Geophysical Research Letters*, 43(15):7946–7952, 2016.

[43] S. Lee, M. F. Wheeler, and T. Wick. Pressure and fluid-driven fracture propagation in porous media using an adaptive finite element phase field model. *Computer Methods in Applied Mechanics and Engineering*, 305:111 – 132, 2016.

[44] S. Lee, M. F. Wheeler, and T. Wick. Iterative coupling of flow, geomechanics and adaptive phase-field fracture including level-set crack width approaches. *Journal of Computational and Applied Mathematics*, 314:40 – 60, 2017.

[45] S. Mandal, A. Ouazzi, and S. Turek. Modified Newton solver for yield stress fluids. In *Numerical Mathematics and Advanced Applications, ENUMATH 2015*. Springer, 2016.

[46] C. Maurini, B. Bourdin, G. Gauthier, and V. Lazarus. Crack patterns obtained by unidirectional drying of a colloidal suspension in a capillary tube: experiments and numerical simulations using a two-dimensional variational approach. *International Journal of Fracture*, 184(1):75–91, 2013.

[47] C. Mehlmann and T. Richter. A modified global newton solver for viscous-plastic sea ice models. *Ocean Modelling*, 116:96 – 107, 2017.

[48] A. Mesgarnejad, B. Bourdin, and M. Khonsari. Validation simulations for the variational approach to fracture. *Computer Methods in Applied Mechanics and Engineering*, 290:420 – 437, 2015.

[49] C. Miehe, M. Hofacker, L.-M. Schaenzel, and F. Aldakheel. Phase field modeling of fracture in multi-physics problems. part ii. coupled brittle-to-ductile failure criteria and crack propagation in thermo-elasticplastic solids. *Computer Methods in Applied Mechanics and Engineering*, 294:486 – 522, 2015.

[50] C. Miehe, M. Hofacker, and F. Welschinger. A phase field model for rate-independent crack propagation: Robust algorithmic implementation based on operator splits. *Comput. Meth. Appl. Mech. Engrg.*, 199:2765–2778, 2010.

[51] C. Miehe, S. Mauthe, and S. Teichtmeister. Minimization principles for the coupled problem of darcybiot-type fluid transport in porous media linked to phase field modeling of fracture. *Journal of the Mechanics and Physics of Solids*, 82:186 – 217, 2015.

[52] C. Miehe, L.-M. Schaenzel, and H. Ulmer. Phase field modeling of fracture in multi-physics problems. part i. balance of crack surface and failure criteria for brittle crack propagation in thermo-elastic solids. *Computer Methods in Applied Mechanics and Engineering*, 294:449 – 485, 2015.

[53] C. Miehe, F. Welschinger, and M. Hofacker. Thermodynamically consistent phase-field models of fracture: variational principles and multi-field fe implementations. *Int. J. Numer. Methods Engrg.*, 83:1273–1311, 2010.

[54] A. Mikelić, M. Wheeler, and T. Wick. Phase-field modeling of pressurized fractures in a poroelastic medium. ICES Report 14-18, Jun 2014.

[55] A. Mikelić, M. F. Wheeler, and T. Wick. A phase-field method for propagating fluid-filled fractures coupled to a surrounding porous medium. *SIAM Multiscale Model. Simul.*, 13(1):367–398, 2015.

[56] A. Mikelić, M. F. Wheeler, and T. Wick. Phase-field modeling of a fluid-driven fracture in a poroelastic medium. *Computational Geosciences*, 19(6):1171–1195, 2015.

[57] A. Mikelić, M. F. Wheeler, and T. Wick. A quasi-static phase-field approach to pressurized fractures. *Nonlinearity*, 28(5):1371–1399, 2015.

[58] P. Mital, T. Wick, M. Wheeler, and G. Pencheva. Discontinuous and enriched galerkin methods for phase-field fracture propagation in elasticity. In *Numerical Mathematics and Advanced Applications, ENUMATH 2015*. Springer, 2016.

[59] J. More and D. Sorensen. On the use of directions of negative curvature in a modified newton method. *Mathematical Programming*, 16:1–20, 1979.

[60] I. Neitzel, T. Wick, and W. Wollner. An optimal control problem governed by a regularized phase-field fracture propagation model. *SIAM Journal on Control and Optimization*, 55(4):2271–2288, 2017.

[61] J. Nocedal and S. J. Wright. *Numerical optimization*. Springer Ser. Oper. Res. Financial Engrg., 2006.

[62] A. Schlüter, A. Willenbücher, C. Kuhn, and R. Müller. Phase field approximation of dynamic brittle fracture. *Comput. Mech.*, 54:1141–1161, 2014.

[63] I. N. Sneddon and M. Lowengrub. *Crack problems in the classical theory of elasticity*. SIAM series in Applied Mathematics. John Wiley and

Sons, Philadelphia, 1969.

[64] H. Ulmer, M. Hofacker, and C. Miehe. Phase field modeling of brittle and ductile fracture. *PAMM*, 13:533–536, 2013.

[65] N. van Goethem and A. Novotny. Crack nucleation sensitivity analysis. *Math. Methods Appl. Sci.*, 33(16), 2010.

[66] C. V. Verhoosel and R. de Borst. A phase-field model for cohesive fracture. *International Journal for Numerical Methods in Engineering*, 96(1):43–62, 2013.

[67] J. Vignollet, S. May, R. Borst, and C. V. Verhoosel. Phase-field models for brittle and cohesive fracture. *Meccanica*, 49(11):2587–2601, 2014.

[68] M. Wheeler, T. Wick, and W. Wollner. An augmented-Lagangrian method for the phase-field approach for pressurized fractures. *Comp. Meth. Appl. Mech. Engrg.*, 271:69–85, 2014.

[69] D. Wick, T. Wick, H. R. Hellmig, and H.-J. Christ. Numerical simulations of crack propagation in screws with phase-field modeling. *Computational Materials Science*, 109:367–379, 2015.

[70] T. Wick. Solving monolithic fluid-structure interaction problems in arbitrary Lagrangian Eulerian coordinates with the deal.II library. *Archive of Numerical Software*, 1:1–19, 2013.

[71] T. Wick. Coupling fluid-structure interaction with phase-field fracture. *Journal of Computational Physics*, 327:67 – 96, 2016.

[72] T. Wick. Goal functional evaluations for phase-field fracture using PU-based DWR mesh adaptivity. *Computational Mechanics*, 57(6):1017–1035, 2016.

[73] T. Wick. An error-oriented Newton/inexact augmented Lagrangian approach for fully monolithic phase-field fracture propagation. *SIAM Journal on Scientific Computing*, 39(4):B589–B617, 2017.

[74] V. Ziaei-Rad and Y. Shen. Massive parallelization of the phase field formulation for crack propagation with time adaptivity. *Computer Methods in Applied Mechanics and Engineering*, 312:224 – 253, 2016. Phase Field Approaches to Fracture.